Summer Student Project: Identification of electrons at the LHCb experiment

Rikke Stougaard Klausen
Masterstudent at the Niels Bohr Institute, University of Copenhagen

Supervised by:
Renato Quagliani and Vava Gligorov

August 2024

Acknowledgments

I would like to thank my supervisors, Renato Quagliani and Vava Gligorov, for their guidance and support throughout this project. Your feedback and advice were invaluable in helping me complete this work, and I appreciate the opportunity to learn from you both. Thank you for making this a positive and rewarding experience.

And of course a huge shout out to my friends at CERN, my partner, and my friends at home. This would not be worth it without you.

Contents

1 Introduction

LHCb is an experiment dedicated to heavy flavour physics at the LHC. Its primary goal is to look for indirect evidence of new physics in CP violation and rare decays of beauty and charm hadrons. The LHCb is a single-arm spectrometer with a forward angular coverage from approximately 10mrad to 300 (250) mrad in the bending (non-bending) plane. The choice of the detector geometry is justified by the fact that at high energies both the b- and b-hadrons are predominantly produced in the same forward or backward cone [2]. The layout of the LHCb spectrometer is shown in Fig. 1.

The project aims to set up fits to calibrate data in 2024 data taking for the LHCb experiment by evaluating the efficiencies of Particle Identification (PID) requirements for electrons and muons using reconstructed $B^+ \to K^+ J/\psi(\ell^- \ell^+)$ decays. These decays are selected such that one of the leptons produced in the J/ψ decay (tag) has a PID requirement applied while the other lepton (probe) does not. The efficiency of PID requirements can then be evaluated on a per-track basis.

By computing the efficiencies in bins of the track kinematics, one can correct simulated samples as a function of the variables used to parameterize the efficiency. For electrons, one important variable is whether or not the electron has an associated bremsstrahlung cluster, since the presence of recovered photons from bremsstrahlung is in itself a powerful discriminant between an electron and other types of particles. The PID corrections derived by this method will determine the $(K^+ J/\psi \to e^- e^+)/(K^+ J/\psi \to \mu^- \mu^+)$ ratio (rKJ/ψ) in 2024 data.

The (rKJ/ψ) test can show how well we can control the efficiency determination of muons and electrons which behave vastly differently in the detector (in particular since electrons produce bremsstrahlung photons, while muons do not). The efficiency determination of electrons is driven by the calorimeter and RICH and for muons from muon-stations. This study only focuses on the PIDe performance of the electrons.

Differently from Run1 and Run2, the Run3 data taking (2024 in our case) is characterized by removing the hardware trigger which, especially for electrons vs muons performance, makes the reconstruction efficiency of decays with electrons in final states similar to muons. Removing this element (hardware trigger) should help to simplify the calibration of efficiencies. In particular, while before one had to convolve the big differences in the trigger, PID, and tracking performance of an electron versus a muon, while now we now expect to correct for PID and tracking only.

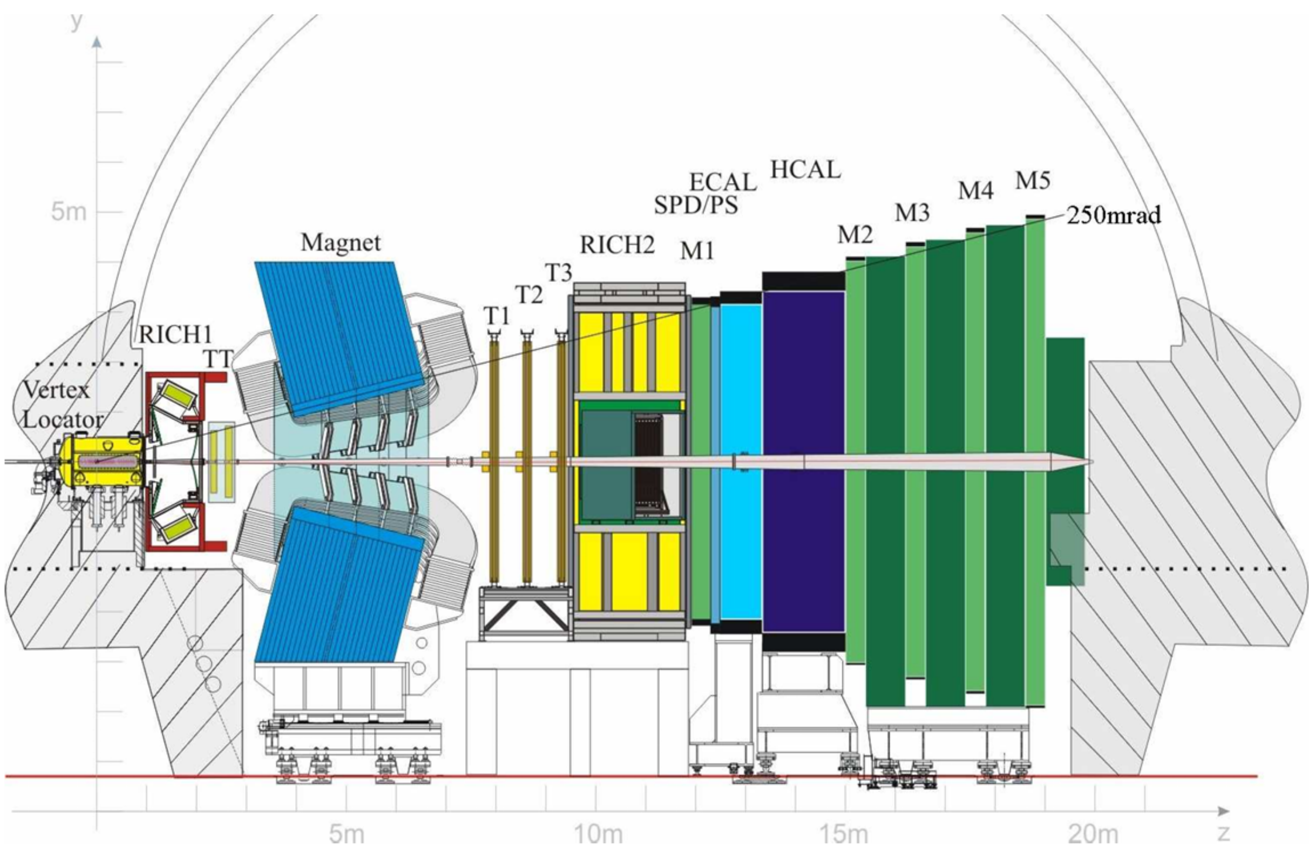

Fig. 1: View of the LHCb detector.

The 2024 data has been taken in different conditions during the year. In particular data taken before the May 2024 Technical Stop (TS) did not have the Upstream Tracker (UT) included in the reconstruction. The majority of post-TS data did include the UT in the reconstruction and various updates in alignment and stability of data taking occurred throughout the year. In addition to their use in physics analysis, the calibration and study of PID responses are crucial to ensure successful analyses and to understand the detector's behavior.

To facilitate this, a fit-in-bins setup is developed for PID calibration. This tool features a flexible interface that enables various types of studies by adjusting the size and number of bins, binning variables, input samples, and sample selections (quality criteria, prior probe criteria), as well as the criteria for efficiency determination. In summary, making variations on the setup allows one to determine different correction schemes, leading to various systematic determinations on the PID calibration for a given dataset.

2 Data and preselection

The data in this analysis are purely done electrons (`"kee_calib_eminus"`, `"kee_calib_eplus"`) from the post-TS period `"data_postts_magdown_turcal"`. The following preselection is the same for every dataset throughout.

```
    "preselection"       : [ "B_BPVFDCHI2              > 100          ",
                             "Jpsi_MAXSDOCACHI2        < 30           ",
                             "Jpsi_PT                  > 0            ",
                             "Jpsi_M                   < 5500         ",
                             "Jpsi_BPVIPCHI2           > 0            ",
                             "Jpsi_END_VCHI2DOF        < 9            ",
                             "B_END_VCHI2DOF           < 9            ",
                             "B_BPVIPCHI2              < 25           ",
                             "B_BPVDIRA                > 0.9995       ",
                             "K_BPVIPCHI2              > 9            ",
                             "E_tag_BPVIPCHI2          > 4            ",
                             "E_tag_INECAL             ==1            ",
                             "E_tag_PID_E              > 3            ",
                             "E_tag_PPHASRICH          ==1            ",
                             "K_ISMUON                 !=1            ",
                             "K_PPHASRICH              ==1            ",
                             "K_PID_K                  > 4            ",
                             "E_probe_K_OA             > 0.0005       ",
                             "E_tag_K_OA               > 0.0005       ",
                             "E_probe_E_tag_OA         > 0.0005       " ]

    "prior_cut"          : [ "E_probe_INECAL==1" , "E_probe_PPHASRICH==1"]
```

The preselection of `"K_PID_K > 4"` is applied to reduce background from the Cabibbo suppressed decay $B^+ \to \pi^+ J/\psi$ making it negligible and not needed to model in the background.

3 Fit setup

This section describes the fit strategy specifying the signal model and backgrounds. This analysis uses `zfit` [5] for one-dimensional maximum extended unbinned likelihood fits on the reconstructed 3-body (B^+) invariant mass from the resonant mode $B^+ \to K^+ J/\psi(e^- e^+)$. The double-sided Crystal Ball (DCB) describes the reconstructed invariant mass distribution. The background is modeled with an analytical exponential function for the *Combinatorial* and a Kernel Density Estimation (KDE) for the *Partially Reconstructed* (PartReco) [1].

The analytical PDFs for the invariant mass of the signal and for some components of the background have many degrees of freedom. When binning the data and applying an PIDe efficiency criterion to split into the binned data into passed and failed samples, the fit in both the passed and failed sample can become unstable if a given bin contains too few events. Therefore, a simulated data signal is fitted beforehand to fix the mean and width of the resonance peak which are shared parameters in the pass-and-fail fit. We introduce two fit parameters for a mass shift, m_{shift}, and width scale s_{scale}.

- $m_{\text{mass}} = m_{\text{MC}} + m_{\text{shift}}$
- $\sigma \to s_{\text{scale}} \cdot \sigma_{\text{MC}}$.

The fitted simulated signal in the pass-and-fail sample is shown in Fig. 2 along with the KDE which describes the PartReco background.

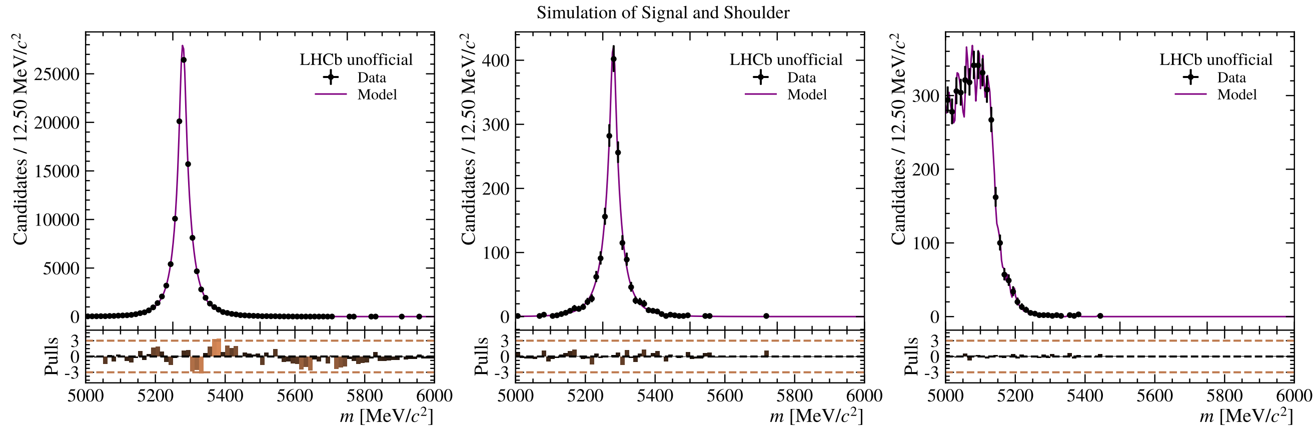

Fig. 2: Fit of simulated passed (left) signal, failed (middle) signal, and PartReco (right).

Since the PartReco is modeled by the KDE with no degrees of freedom the fit only returns a yield. The yield can be used to compute the ratio of the PartReco to the signal, which is subsequently shared between the passed and failed samples,

$$N_{\text{PartReco,fail}} = N_{\text{sig,fail}} \frac{N_{\text{PartReco,pass}}}{N_{\text{sig,pass}}}. \tag{1}$$

By fitting the passed and failed samples simultaneously the efficiency, ε, of a criterion can be extracted directly from the fitting procedure. Since

$$\frac{N_{\text{sig,pass}}}{N_{\text{sig,total}}} = \frac{N_{\text{sig, pass}}}{N_{\text{sig, pass}} + N_{\text{sig, fail}}} = \varepsilon, \tag{2}$$

and by making the failed signal yield a composed parameter of the passed signal yield and the efficiency; the efficiency can be treated as a fit parameter:

$$N_{\text{sig,fail}} = \frac{N_{\text{sig,pass}}(1-\varepsilon)}{\varepsilon}. \tag{3}$$

4 Analysis

The tool bins the data directly in ROOT [4] and splits every bin data into a passed and failed sample determined by the PID criterion. This section describes how variations of the setup affect the quality of the data to fit, and what to be aware of in the binning scheme. The first part is on further prior criteria for quality of data and the second part is on low statistics in bins.

4.0.1 Further prior criteria

To create passed and failed samples we must choose our dataset and define our criterion for efficiency.

```
    "data"                  : "kee_calib_eminus"
    "cuts_for_efficiency" : { "24_postts_magdown_eminus_PID_E_2" : "E_probe_PID_E > 2"}
```

The fitted preselected pass and fail sample of a "E_probe_PID_E>2" efficiency criterion is shown in Fig. 3a. A clear signal peak is seen in the passed sample however, the failed sample seems to have a signal peak, but it is tiny compared to the amount of background. This large background presence complicates the determination of the signal within the failed sample. To reduce the amount of background a further prior criterion of "E_probe_PID_E>-5" is added and shown in Fig. 3b.

This step is crucial in refining the PIDe calibration, as it removes extraneous background noise that could otherwise lead to inaccuracies in efficiency determination. By removing these less relevant events, the analysis becomes more robust, allowing for a clearer distinction between signal and background, which in turn improves the reliability of the overall PID calibration process.

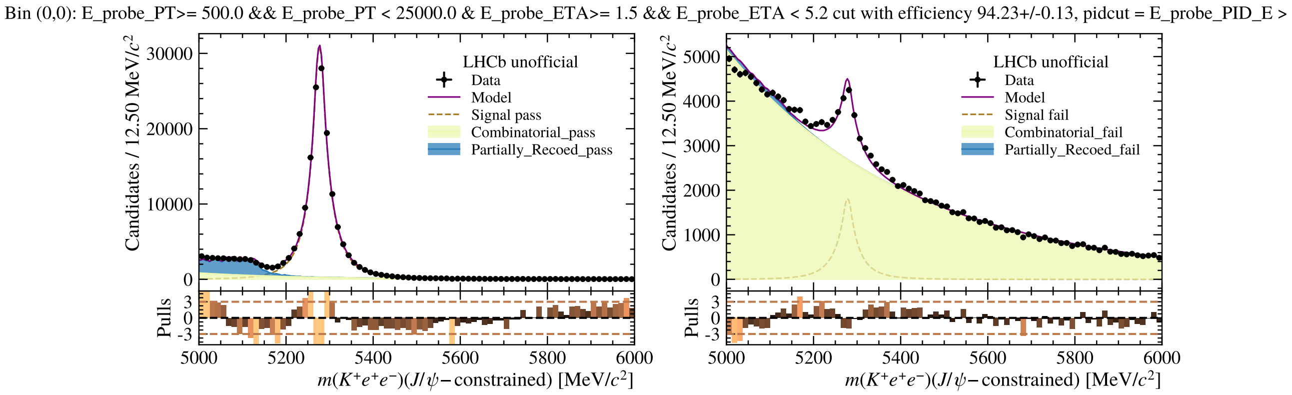

(a) Pass (left) and fail (right) sample without a prior PIDe criterion.

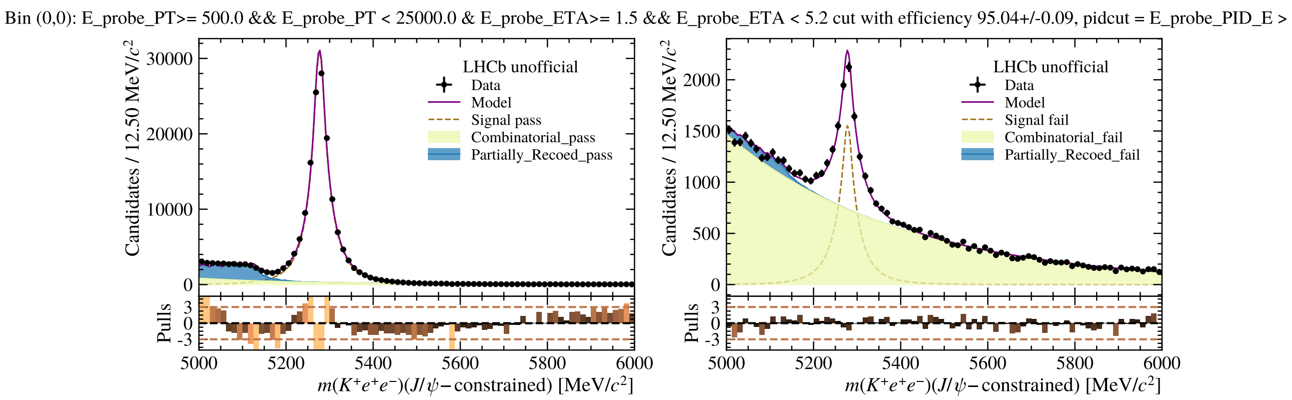

(b) Pass (left) and fail (right) sample with a prior "E_probe_PID_E>-5" criterion.

Fig. 3: Comparison of pass and fail samples with and without a prior PIDe criterion.

4.0.2 Low statistics in bins

We added a prior PID criterion from the previous section to reduce the background, and as an example, we fit in bins of transverse momentum and pseudo-rapidity. For this example, we analyze 20 bins (5 bins in transverse momentum and 4 in psuedo-rapidity).

```
    "binning" : {
          "var1_binning" : {
               "var_name" : "E_probe_PT",
               "linear" : [ 500, 200000, 10],
               "custom" : [ 500.0, 700.0, 2500.0, 4000.0, 9000.0, 25000.0],
               "use" : "custom"},
          "var2_binning" : {
               "var_name" : "E_probe_ETA",
               "linear" : [ 1.5, 5.2, 10],
               "custom" : [ 1.5, 2.5, 3.1, 3.8, 5.2],
               "use" : "custom"}
```

The tool creates a log with the fit results and a PDF file that shows plots of the pass-and-fail fit in every bin for control. Binning the data and splitting the binned data into a pass and final sample statistics can run low. Two fits for the bins (4,2) and (4,3) are shown in Fig. 4 the rest of the fit-in-bins are shown in Appendix A. The failed samples in bins that are shown in Fig. 4 both have low statistics, especially bin (4,3) in Fig. 4b.

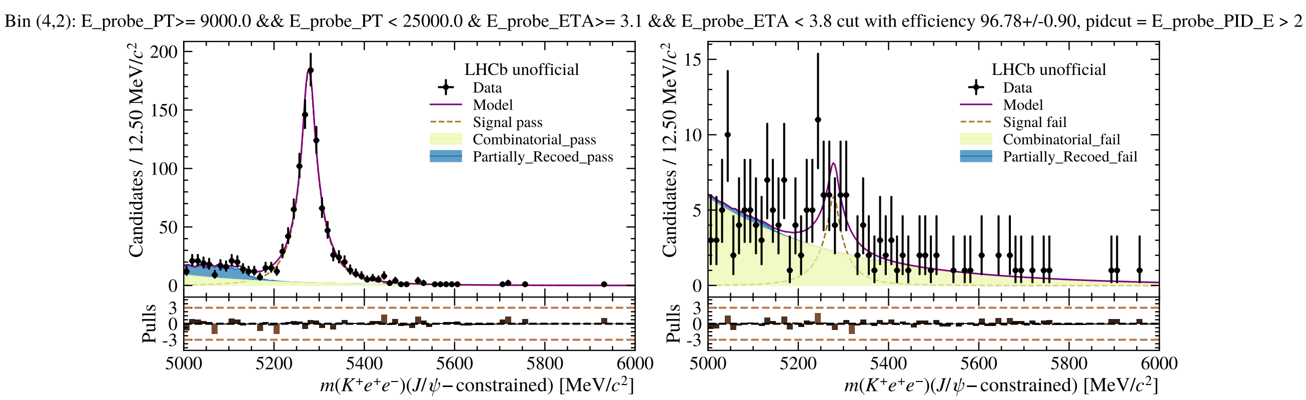

(a) Pass (left) and fail (right) sample of bin (4,2).

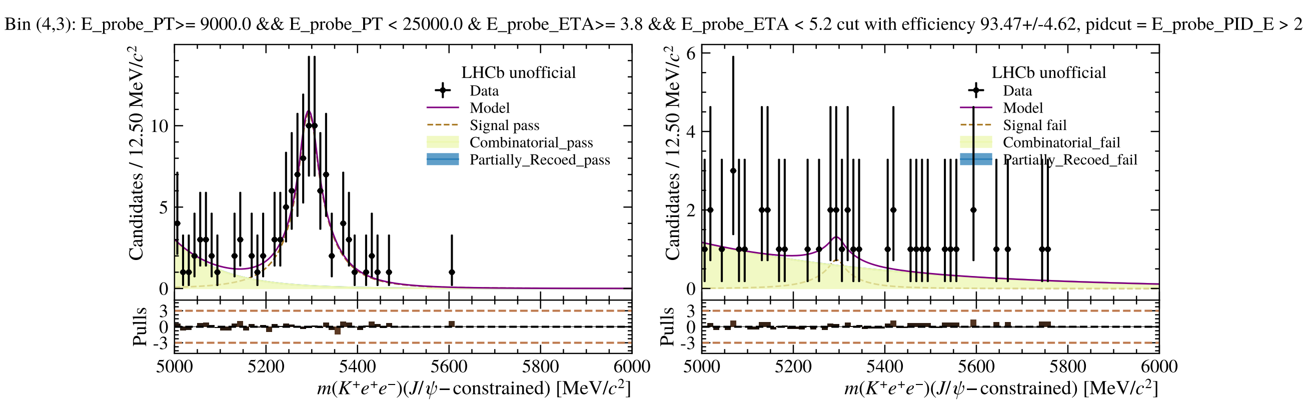

(b) Pass (left) and fail (right) sample of bin (4,3).

Fig. 4: Pass and fail samples with a prior "E_probe_PID_E>-5" criterion of selected bins (4,2) and (4,3) running low in statistics.

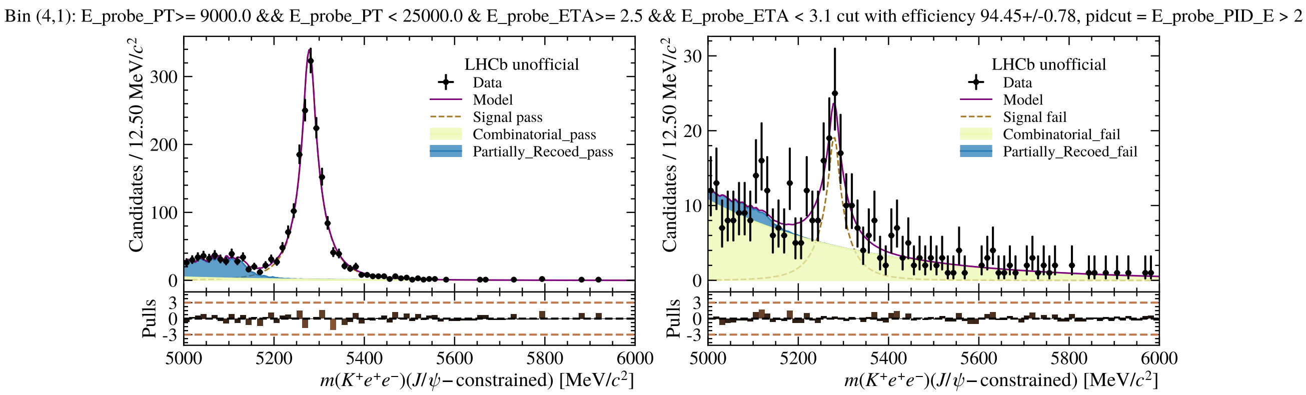

(a) Pass (left) and fail (right) sample of bin (4,1).

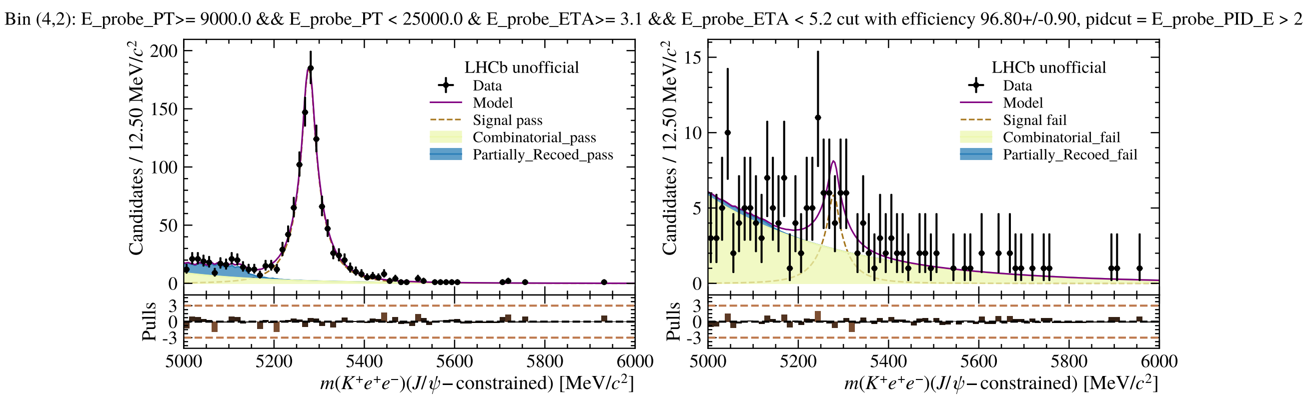

(b) Pass (left) and fail (right) sample of bin (4,2).

Fig. 5: Pass and fail samples with a prior "`E_probe_PID_E>-5`" criterion of selected bins (4,1) and (4,2). This analysis has automatically merged the last two pseudo-rapidity bins due to low statistics as shown in Fig. 4. Data is e^- as probe from the period "postts_magdown_turcal".

To address the issue of low statistics, two bins can be merged into one, although the tool currently does not support manual merging of individual bins. However, it does have the capability to automatically detect low statistics in individual bins based on arbitrary thresholds and merge them with the adjacent bin that has the lowest statistics. This means the tool checks in both variable binning ("`var1_binning`", "`var2_binning`") and merges the lowest statistics bin, and updates the bin edges. For this example, the lowest adjacent bin to the bin (4,3) is bin (4,2) in the pseudo-rapidity ("`var2_binning`") binning scheme. The bin edges for pseudo-rapidity are automatically updated to `[ 1.5, 2.5, 3.1, 5.2]` and now we have 15 bins (5 in transverse momentum and 3 in pseudo-rapidity). The fit-in-bins for the 15 bins are shown in Appendix B.

5 Efficiency plots

Figure 6 presents a 2D histogram that shows the binned efficiency, along with plots for each respective bin. As illustrated in Figure 6b, the analysis reveals a clear trend: the detector's efficiency is highest at higher transverse momentum values but decreases at very high momenta. This decline in efficiency is primarily due to particles with high pseudo-rapidity, which are more likely to be forward-boosted. The area closest to the beamline has more background leading to reduced efficiency in the Inner Electromagnetic Calorimeter (ECAL)[3].

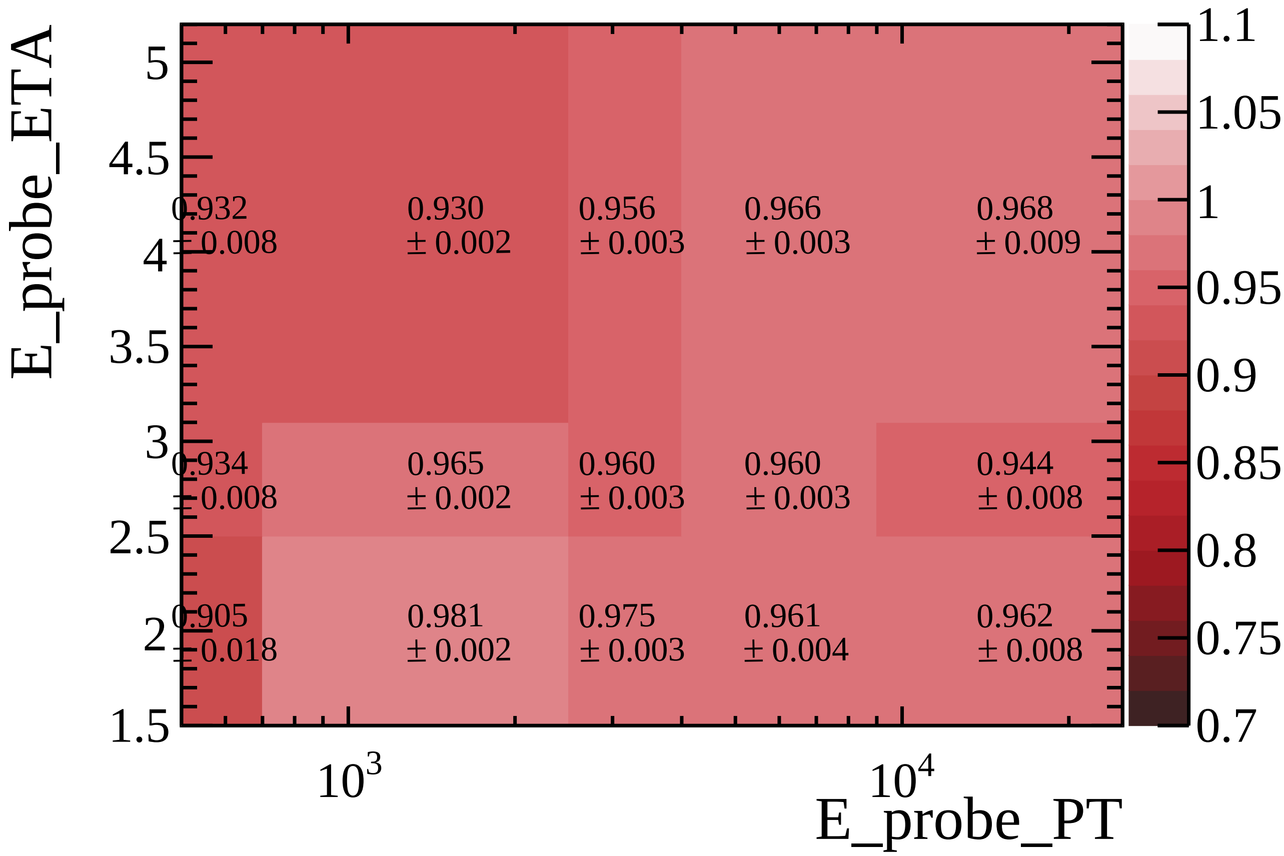

(a) 2D histogram for the efficiency per bin.

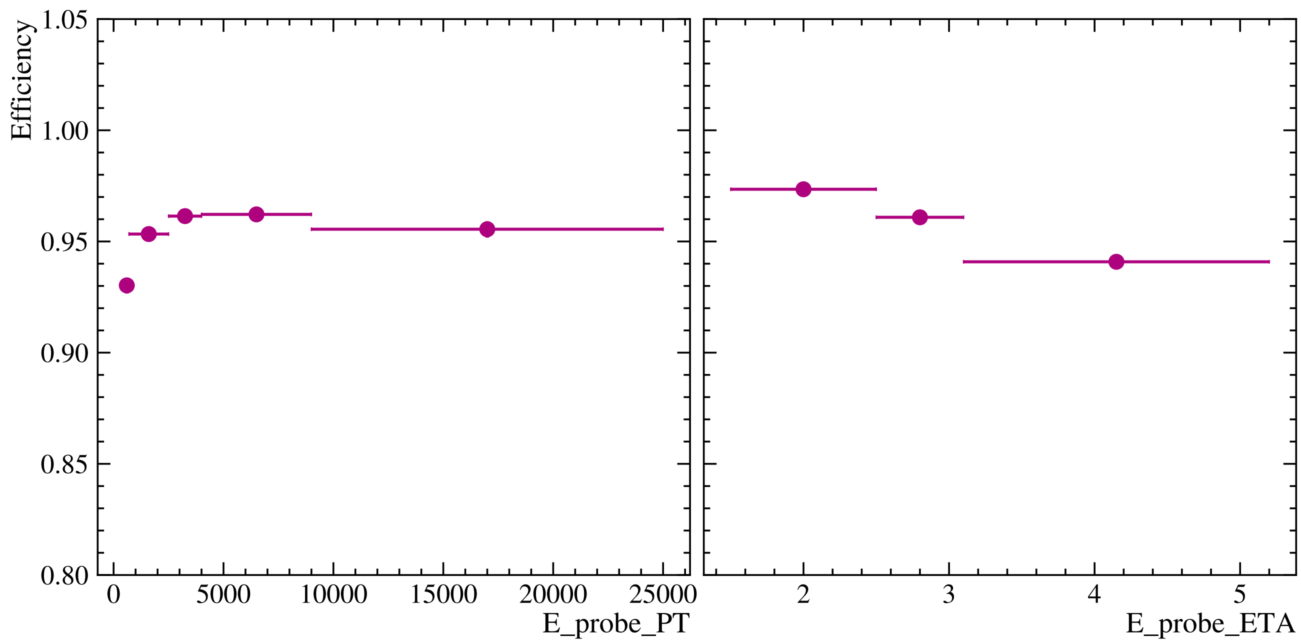

(b) Plots of projected efficiencies onto each binning scheme.

Fig. 6: Efficiency histogram and plots with prior `"E_probe_PID_E>-5"` criterion and efficiency criterion `"E_probe_PID_E>2"`.

5.1 Post-TS analysis on electrons and positrons

The following analysis shows the difference of PIDe efficiency criteria for electrons and positrons in the Post-TS period. The same analysis is performed over the electron and positron data samples. Three efficiency PIDe criteria are chosen to see how loose/tight the detector can identify electrons/positrons. Furthermore, the analysis will include how the PIDe criterion efficiency depends on electrons/positrons with and without associated bremsstrahlung (BREM) photons.

5.1.1 Combined BREM varying PIDe

This analysis does not include a prior BREM selection (`"E_probe_HASBREM"`) which means this data is performed on electrons/positrons with and without BREM. The results in Fig. 7 show that the efficiency decreases with tighter PIDe criteria for both electrons and positrons in both binning schemes. The efficiency for electrons and positrons looks the same.

```
    "prior_cut"            : [ "E_probe_INECAL==1" , "E_probe_PPHASRICH==1" , "E_probe_PID_E > -5"]
```

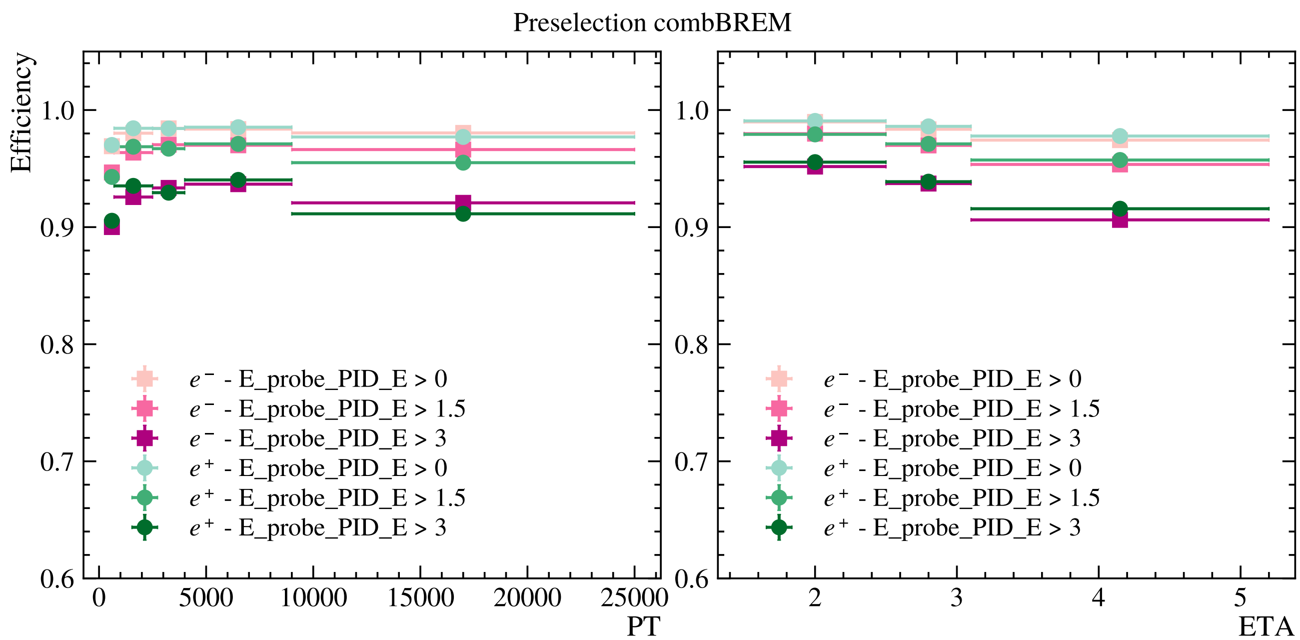

Fig. 7: No `"E_probe_HASBREM"` prior criterion varying PIDe criterion for e^- vs e^+.

5.1.2 Without BREM varying PIDe

This analysis is performed only on electrons and positrons without associated BREM photons. The results in Fig. 8 show an overall decrease in efficiency for both binning variables compare to the results in Fig. 7. The efficiency for electrons is slightly higher than positrons at high transverse momentum, and the opposite is seen in pseudo-rapidity.

```
    "prior_cut"            : [ "E_probe_INECAL==1" , "E_probe_PPHASRICH==1",
                               "E_probe_PID_E > -5", "E_probe_HASBREM==0"]
```

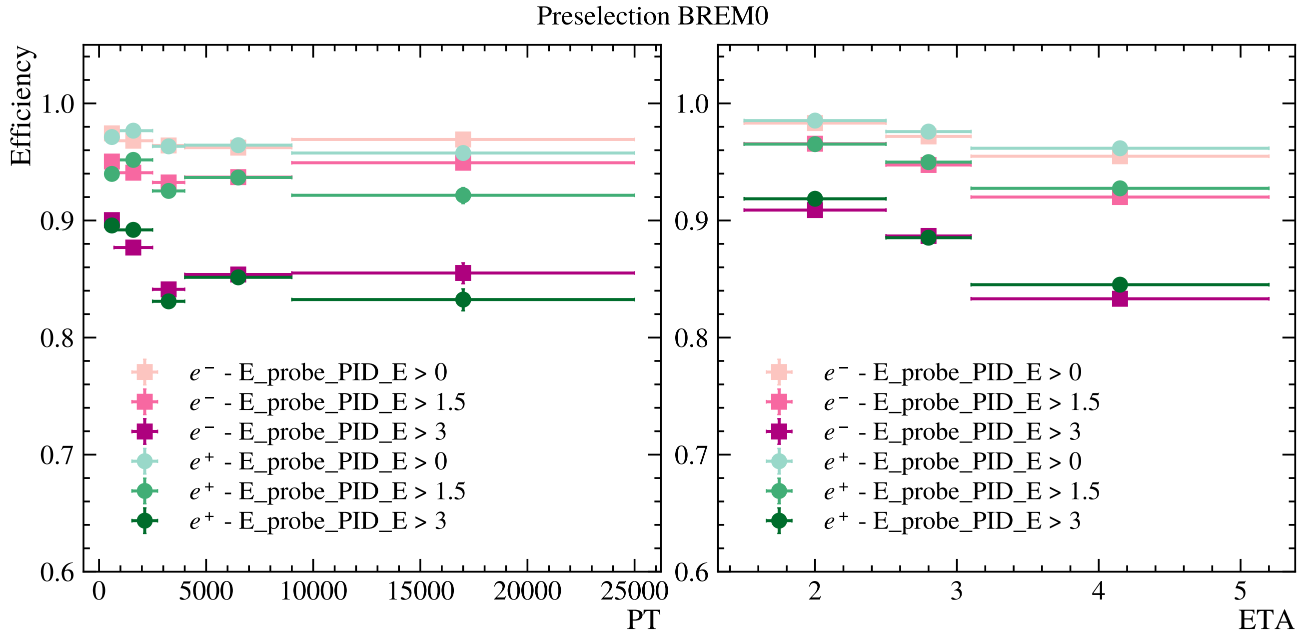

Fig. 8: "E_probe_HASBREM==0" prior criterion varying PIDe criterion for e^- vs e^+.

5.1.3 With BREM varying PIDe

This analysis is performed only on electrons and positrons with associated BREM photons. The results in Fig. 9 and Fig. 10 show an overall increase in efficiency for both binning variables compared to the results without BREM in Fig. 8. Due to low statistics in the failed bin for looser PIDe criteria, the fit-in-bins for "E_probe_PID_E > 0" and "E_probe_PID_E > 1.5" (see Appendix C and D) required a lower statistical threshold to allow data splitting. Without this adjustment, all bins would have been merged into one. However, with this lower threshold, the fit-in-bins produced efficiency results, but the fits were visibly poor. As a result, the data in Fig. 10 do not align with the results for the tighter criterion "E_probe_PID_E > 3" shown in Fig. 9, which had better statistics (see Appendix E).

```
    "prior_cut"          : [ "E_probe_INECAL==1" , "E_probe_PPHASRICH==1",
                             "E_probe_PID_E > -5", "E_probe_HASBREM==1"]
```

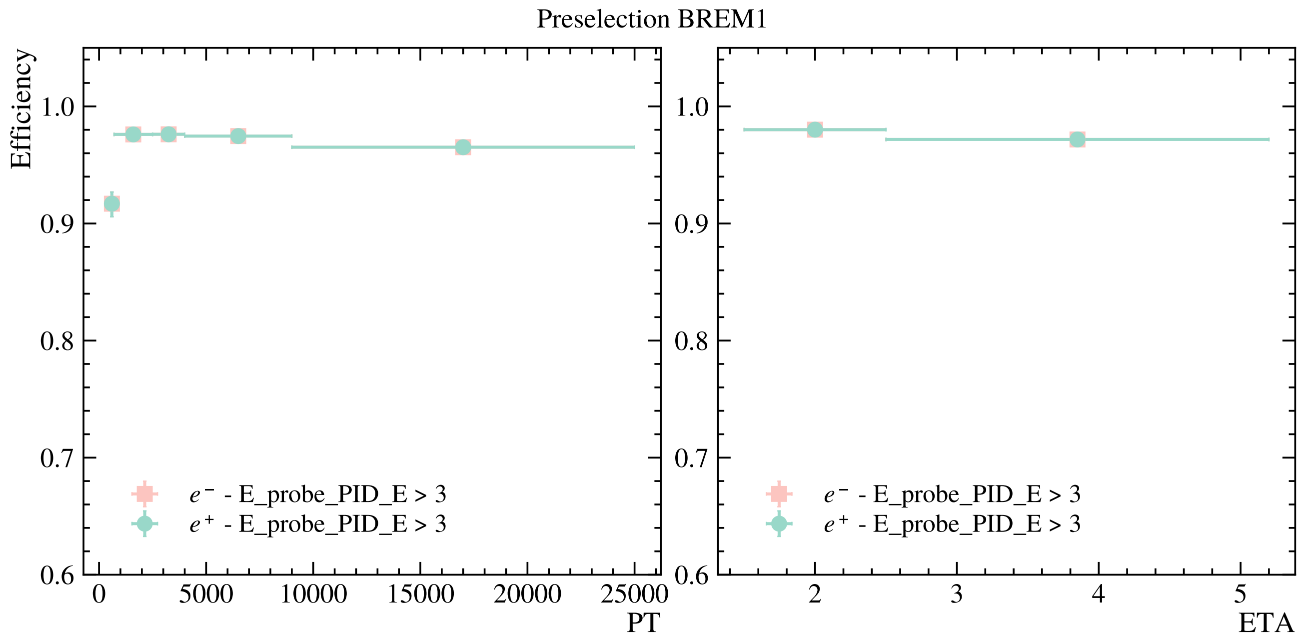

Fig. 9: "E_probe_HASBREM==1" prior criterion with "E_probe_PID_E>3" PIDe criterion for e^- vs e^+.

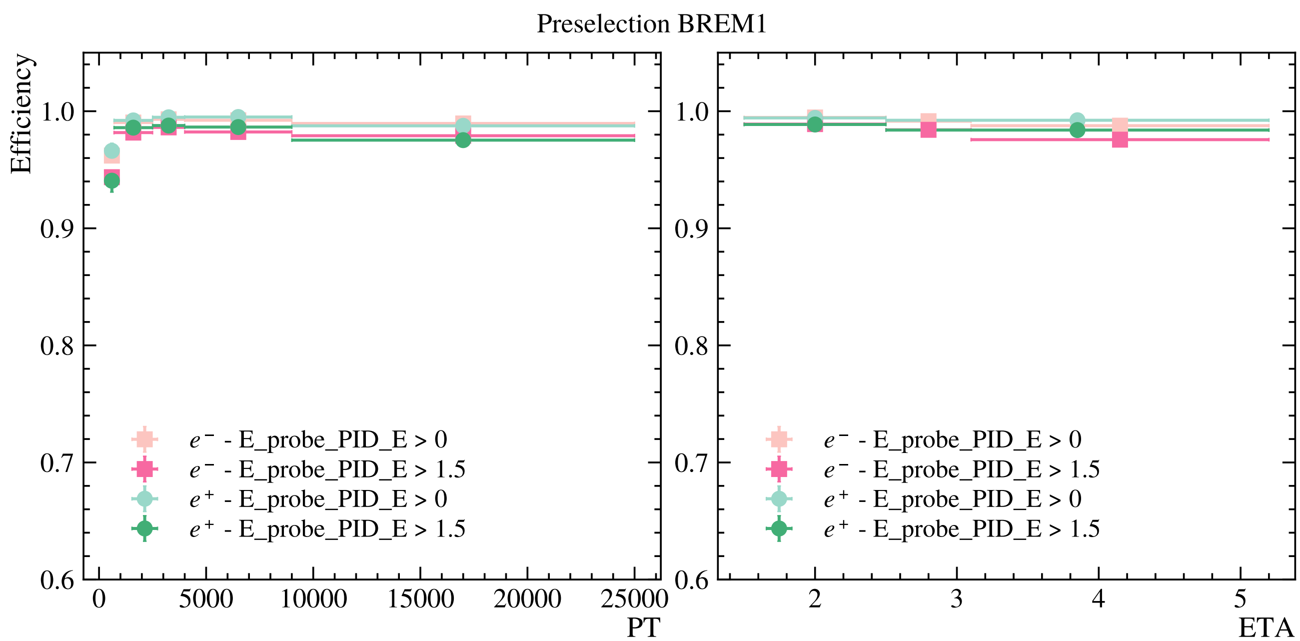

Fig. 10: Low statistics results for "E_probe_HASBREM==1" prior criterion "E_probe_PID_E>0" and "E_probe_PID_E>1.5" PIDe criterion for e^- vs e^+.

5.1.4 PIDe varying BREM

This section demonstrates how the PIDe criterion's efficiency is influenced by the preceding BREM criterion. The results in Figures 11 and 12 indicate that the "E_probe_PID_E>0" criterion is not significantly affected by the prior BREM selections.

In contrast, the tighter criteria "E_probe_PID_E>1.5" and "E_probe_PID_E>3", shown in Figures 13, 14 and 15, reveal that the PIDe efficiency improves when BREM is recovered, compared to when it is not.

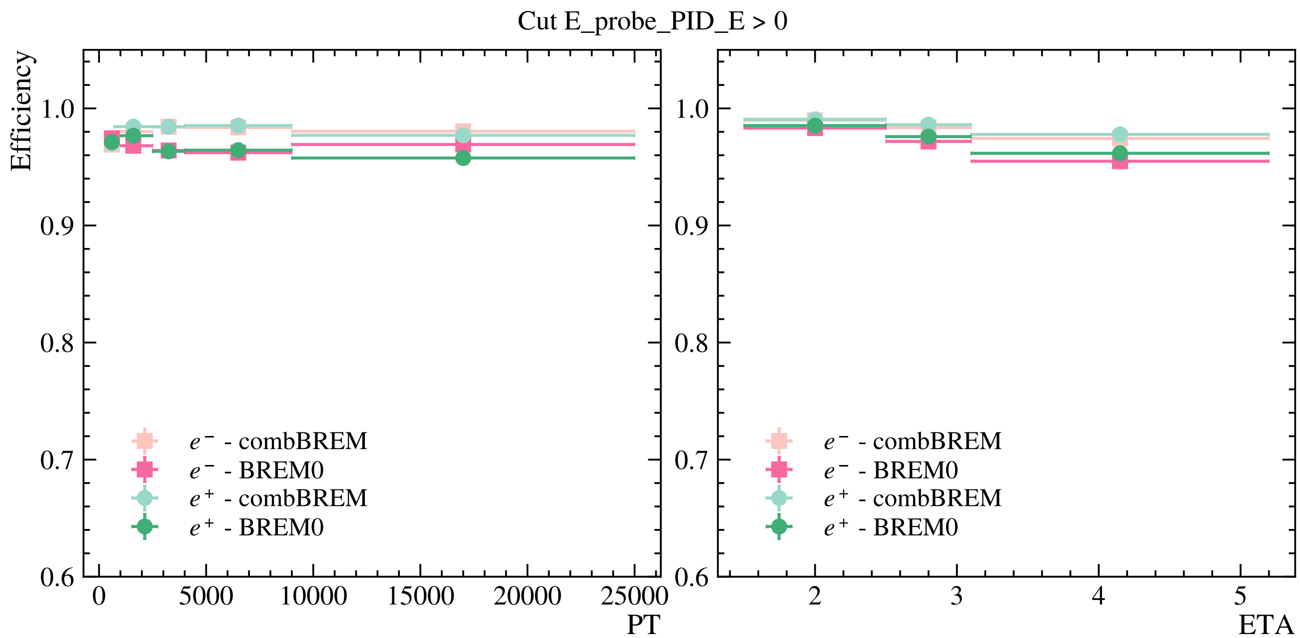

Fig. 11: "E_probe_PID_E>0" criterion varying BREM prior criterion for e^- vs e^+.

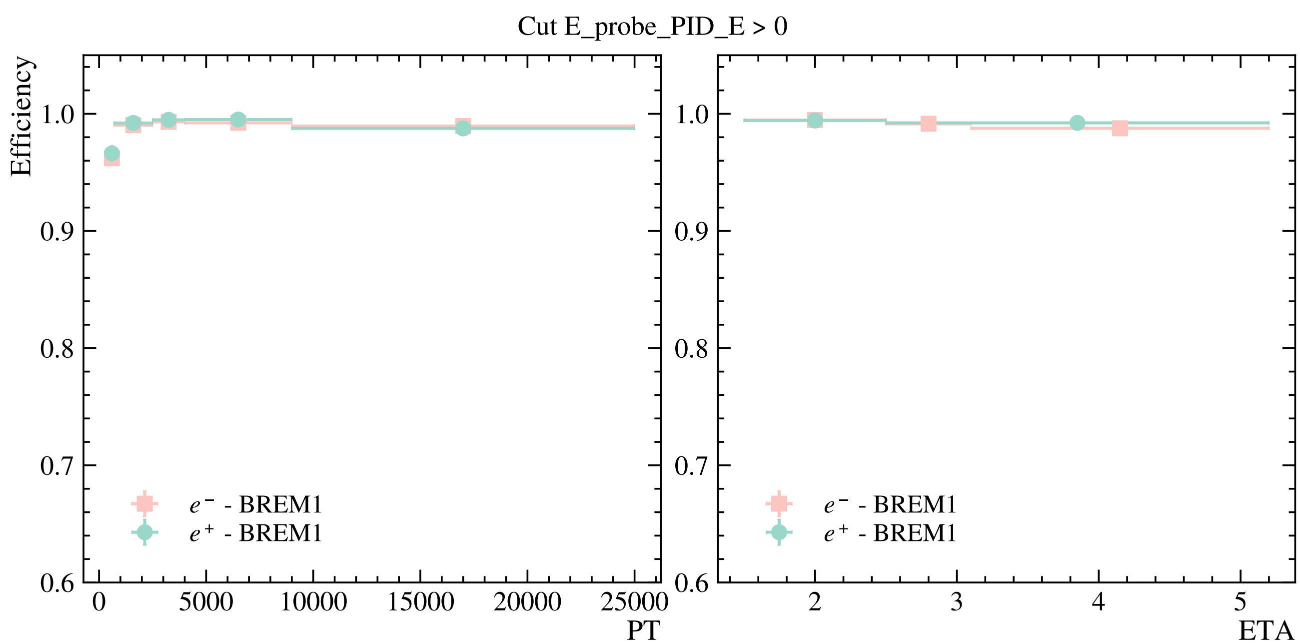

Fig. 12: Low statistics results of "E_probe_PID_E>0" criterion for "E_probe_HASBREM==1" prior criterion of e^- vs e^+.

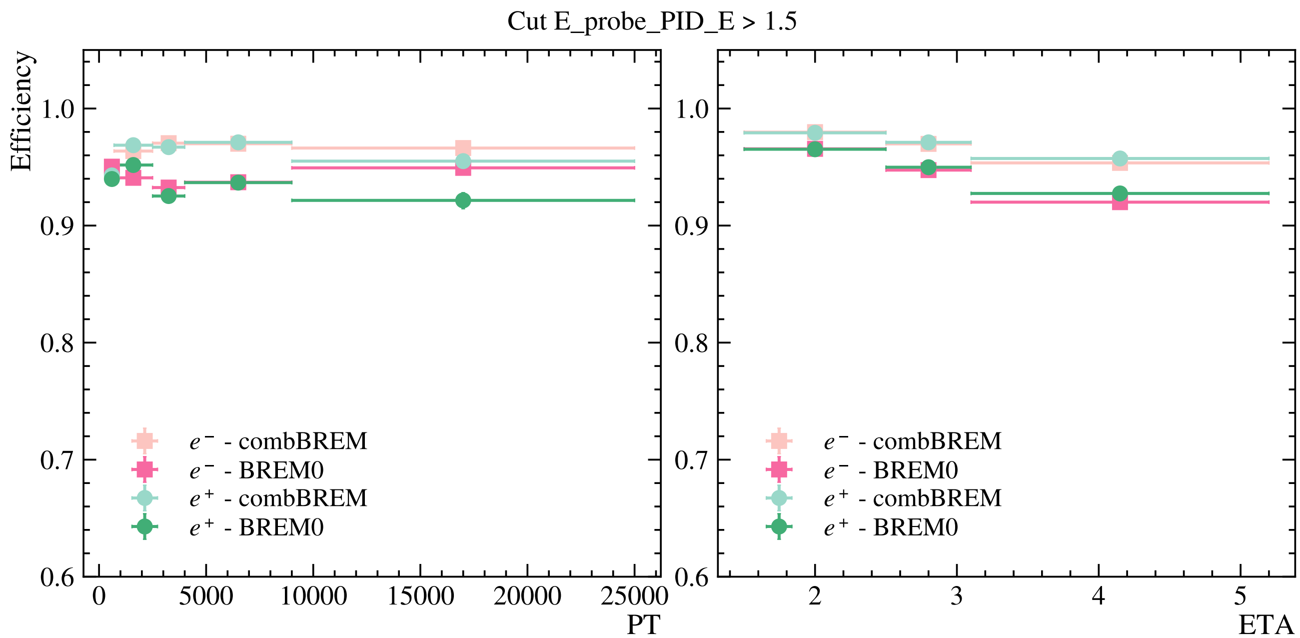

Fig. 13: "E_probe_PID_E>1.5" criterion varying BREM prior criterion for e^- vs e^+.

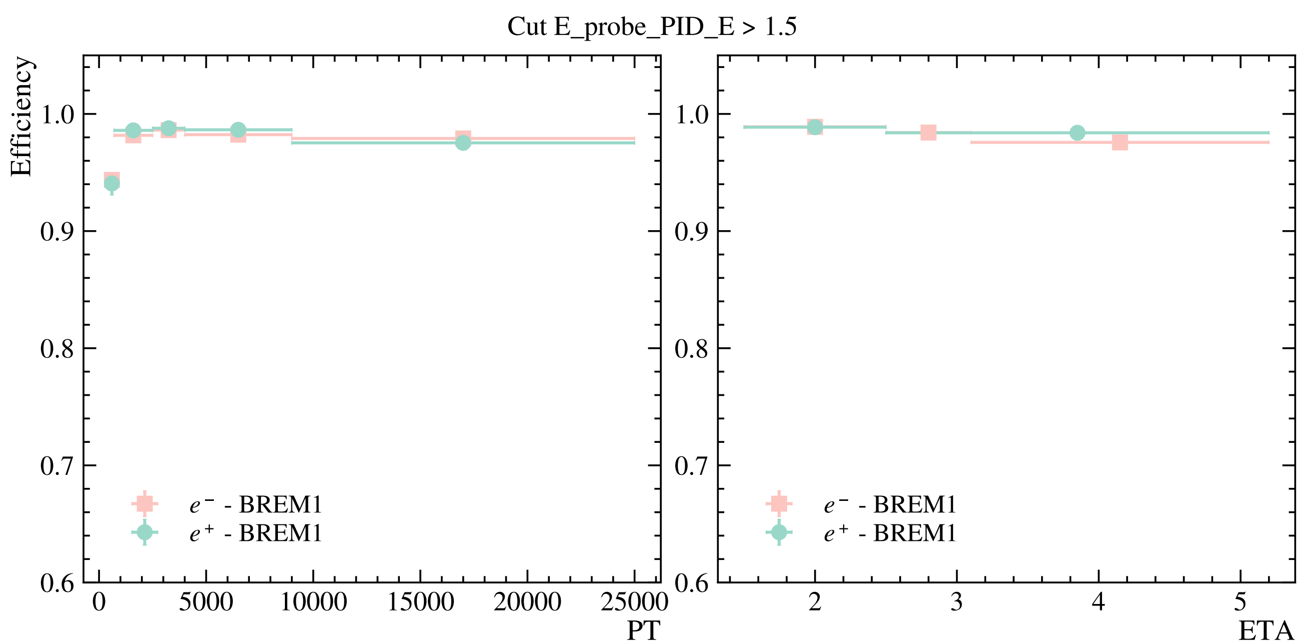

Fig. 14: Low statistics results of "E_probe_PID_E>1.5" criterion for "E_probe_HASBREM==1" prior criterion of e^- vs e^+.

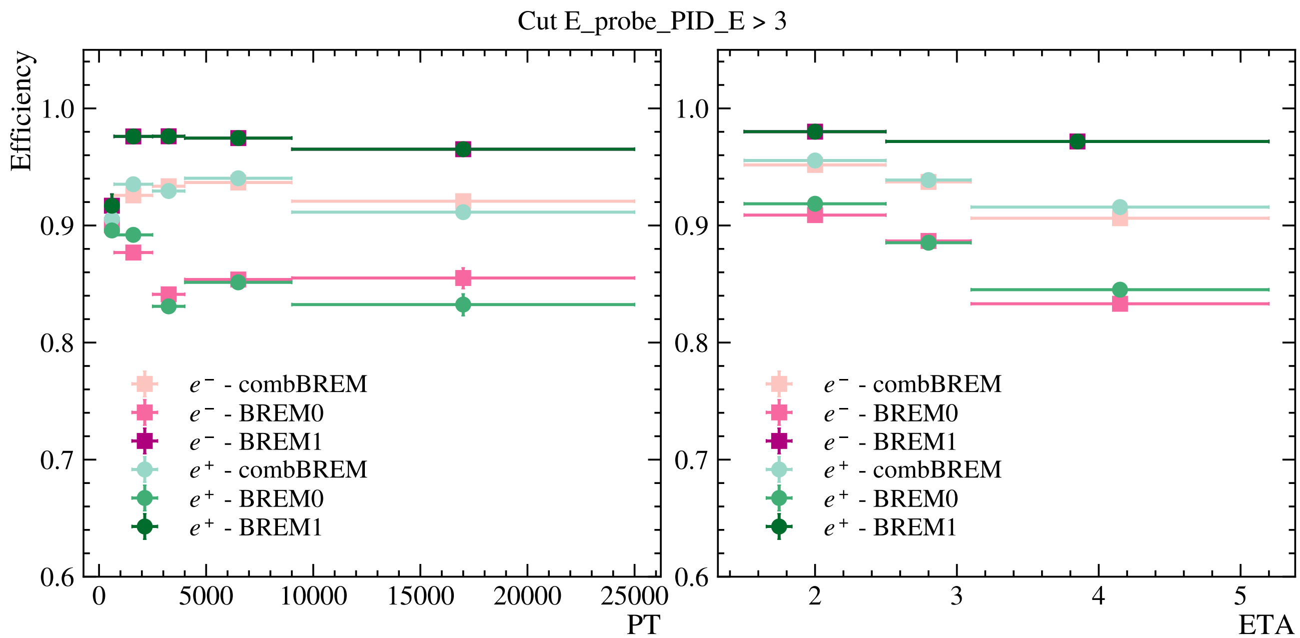

Fig. 15: "E_probe_PID_E>3" criterion varying BREM prior criterion for e^- vs e^+.

6 Conclusion

The analysis presented in these sections provides insight into the detector's efficiency under varying conditions. Initially, the results demonstrate that the detector achieves its highest efficiency at higher transverse momentum, though this efficiency declines at very high momentum due to increased background from forward-boosted particles with high pseudo-rapidity, particularly affecting the Inner Electromagnetic Calorimeter (ECAL).

In the subsequent analysis, the influence of the BREM criterion on the efficiency of the PIDe selection was investigated. It was observed that the basic "E_probe_PID_E>0" criterion remains efficient even without prior BREM selection, particularly for looser PIDe criteria. However, when more stringent PIDe criteria are applied ("E_probe_PID_E>1.5" and "E_probe_PID_E>3"), the efficiency improves significantly when BREM recovery is employed.

Overall, these findings suggest that while the PIDe criterion can be effective without BREM selection for looser thresholds, incorporating BREM recovery becomes increasingly important for maintaining efficiency as the criteria tighten. This insight underscores the need to balance transverse momentum considerations and BREM handling to optimize detector performance in high-background environments.

7 Future work

- Proper implementation of a statistics check
- Run the same analysis with muons $K^+J/\psi \to \mu^-\mu^+$
- Run the machinery for magup/down and pre/post TS to compare performance to understand if we can merge the plus and minus samples and up/down one is compatible.

```
    "period"              : "data_prets_magup_turcal", "data_postts_magup_turcal"
```

- Further studies on the performance of e.i. electron PID in other bin variables than transverse momentum and pseudo-rapidity, but with the ECAL in x and y, and different regions in the ECAL

References

[1] Johannes Albrecht, Simone Bifani, Julian Alexander Boelhauve, Ryan Bernard Calladine, Fabrice Desse, Stephan Escher, Vladimir Gligorov, Christoph Michael Langenbruch, Vitalii Lisovskyi, Simon Nieswand, Francesco Polci, Renato Quagliani, Marie-Helene Schune, Alex Seuthe, Eluned Anne Smith, Da Yu Tou, Nigel Watson, Clotilde Lemettais, Razvan-Daniel Moise, Biljana Mitreska, Lesya Shchutska, and Sebastian Schmitt. Test of lepton flavour universality with $b \to s\ell^+\ell^-$ decays. 2020. URL https://cds.cern.ch/record/2745141.

[2] A. Alves et al. The LHCb Detector at the LHC. *JINST*, 3:S08005, 2008. doi: 10.1088/1748-0221/3/08/S08005. URL https://cds.cern.ch/record/1129809. Also published by CERN Geneva in 2010.

[3] Yasmine Sara Amhis, Carla Marin Benito, and Miriam Calvo Gomez. State of the art of the Run 1 and 2 calorimeter reconstruction and towards the Upgrade. Technical report, CERN, Geneva, 2019. URL https://cds.cern.ch/record/2704284.

[4] Rene Brun and Fons Rademakers. ROOT [software], 2019. URL https://root.cern.ch/. Release v6.18/02, 23/08/2019.

[5] Jonas Eschle, Albert Puig Navarro, Rafael Silva Coutinho, and Nicola Serra. zfit: Scalable pythonic fitting. *SoftwareX*, 11:100508, 2020. ISSN 2352-7110. doi: https://doi.org/10.1016/j.softx.2020.100508. URL https://www.sciencedirect.com/science/article/pii/S2352711019303851.

8 Appendix A

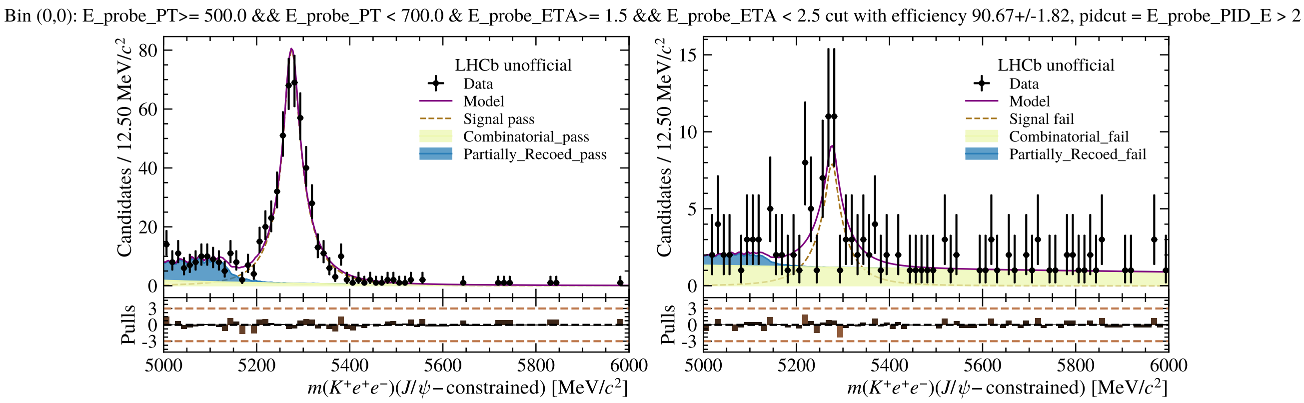

Fig. 16: Fit inbinx-axis-idx=0,y-axis-idx=0

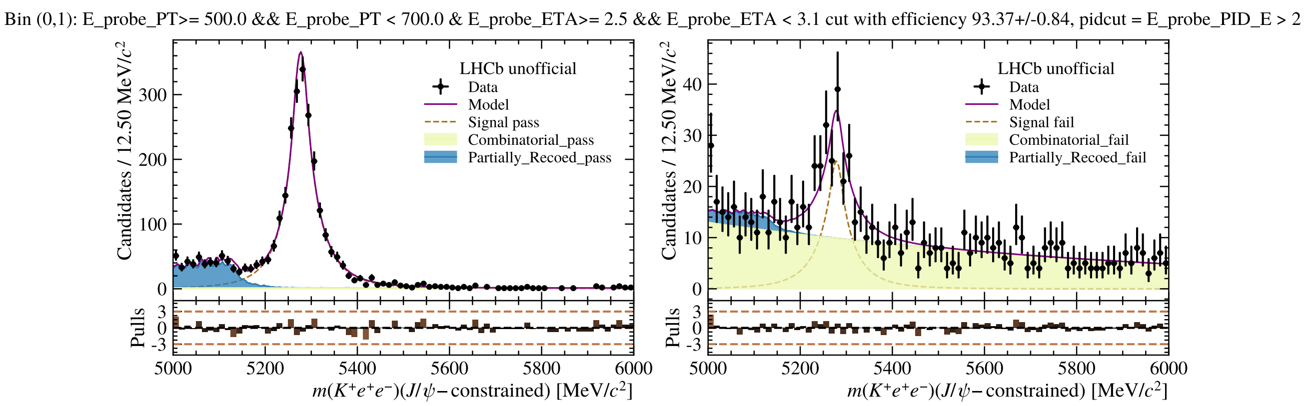

Fig. 17: Fit inbinx-axis-idx=0,y-axis-idx=1

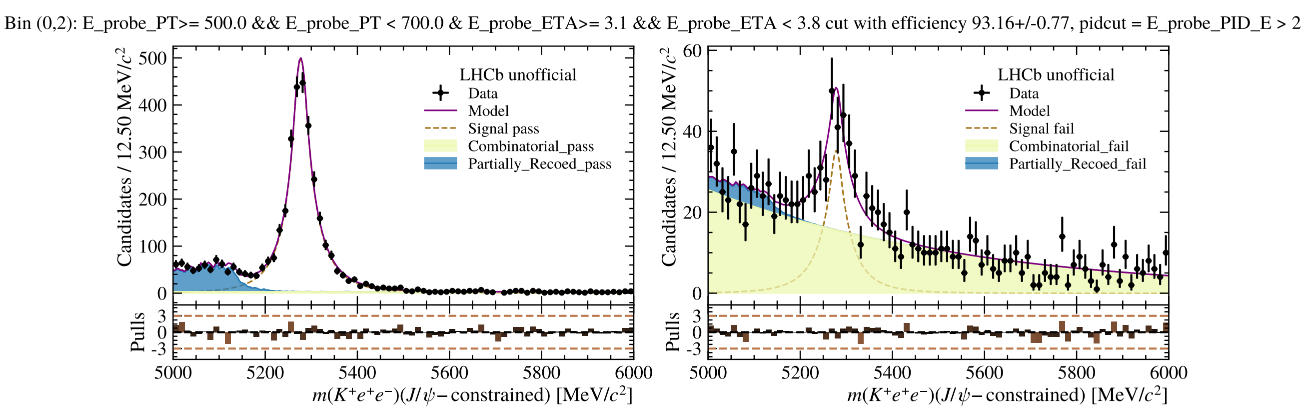

Fig. 18: Fit inbinx-axis-idx=0,y-axis-idx=2

Bin (0,3): E_probe_PT>= 500.0 && E_probe_PT < 700.0 & E_probe_ETA>= 3.8 && E_probe_ETA < 5.2 cut with efficiency 85.99+/-1.38, pidcut = E_probe_PID_E > 2

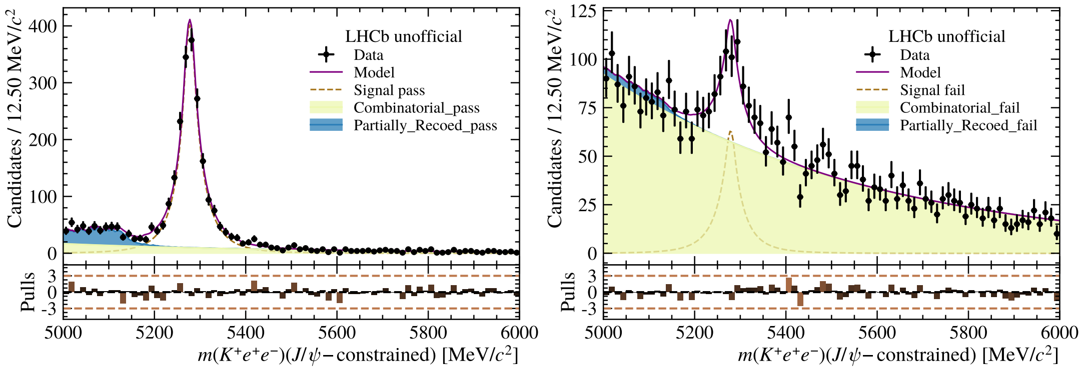

Fig. 19: Fit inbinx-axis-idx=0,y-axis-idx=3

Bin (1,0): E_probe_PT>= 700.0 && E_probe_PT < 2500.0 & E_probe_ETA>= 1.5 && E_probe_ETA < 2.5 cut with efficiency 98.13+/-0.18, pidcut = E_probe_PID_E > 2

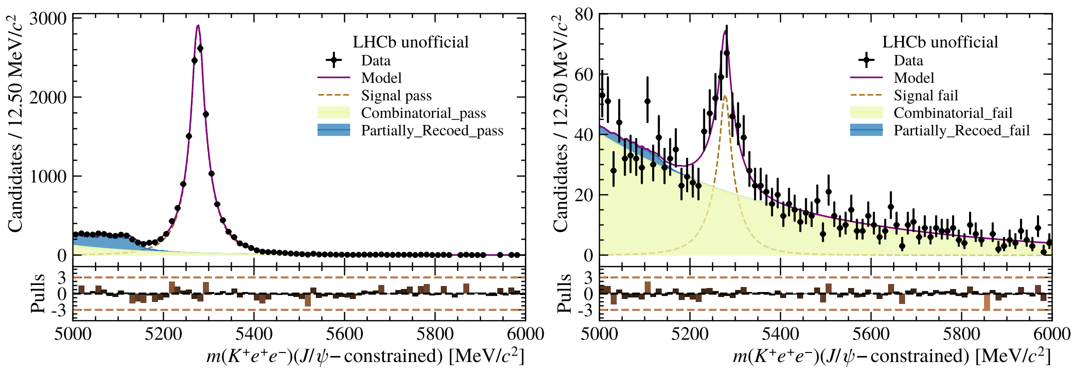

Fig. 20: Fit inbinx-axis-idx=1,y-axis-idx=0

Bin (1,1): E_probe_PT>= 700.0 && E_probe_PT < 2500.0 & E_probe_ETA>= 2.5 && E_probe_ETA < 3.1 cut with efficiency 96.46+/-0.18, pidcut = E_probe_PID_E > 2

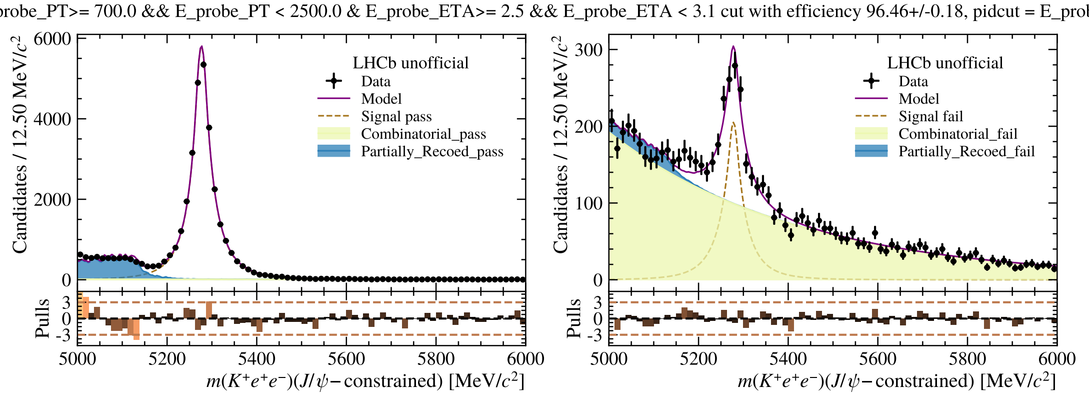

Fig. 21: Fit inbinx-axis-idx=1,y-axis-idx=1

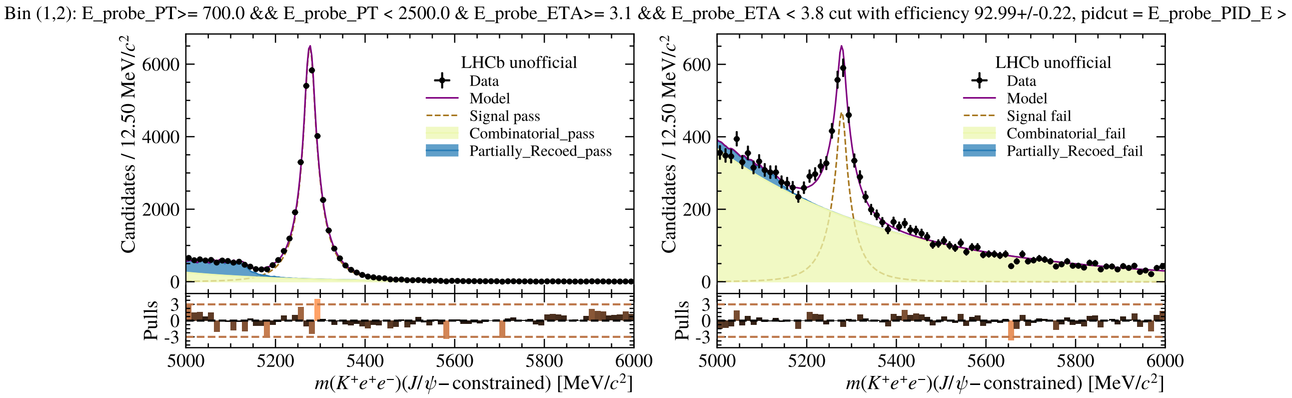

Fig. 22: Fit inbinx-axis-idx=1,y-axis-idx=2

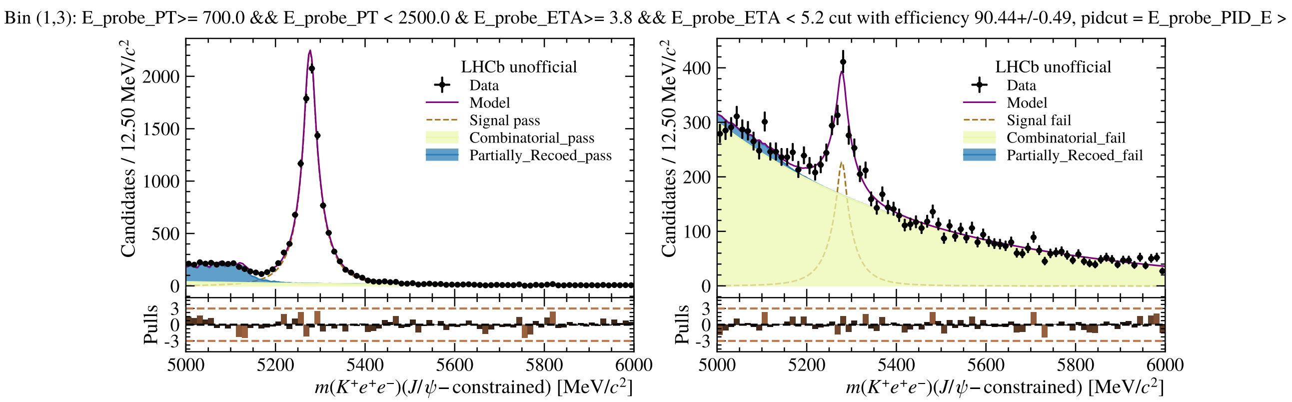

Fig. 23: Fit inbinx-axis-idx=1,y-axis-idx=3

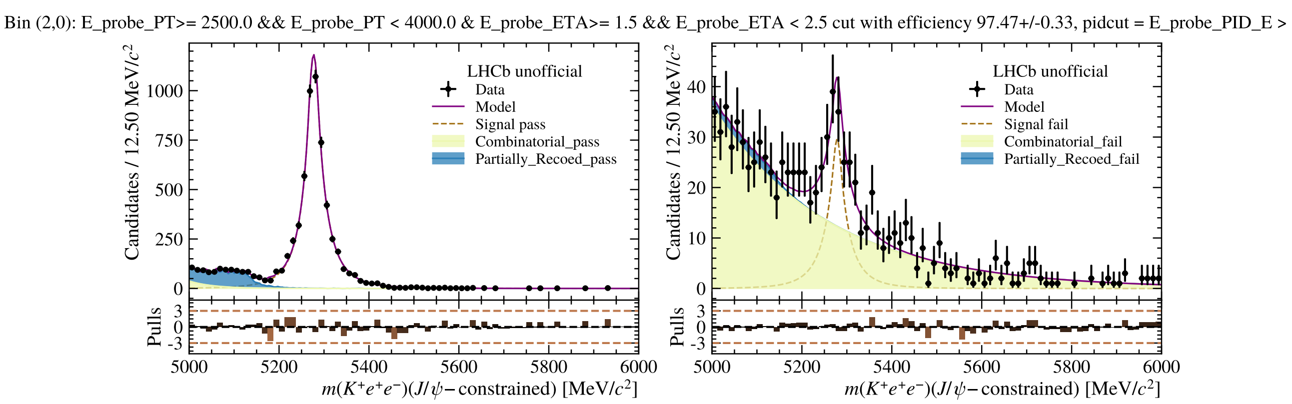

Fig. 24: Fit inbinx-axis-idx=2,y-axis-idx=0

Bin (2,1): E_probe_PT>= 2500.0 && E_probe_PT < 4000.0 & E_probe_ETA>= 2.5 && E_probe_ETA < 3.1 cut with efficiency 95.96+/-0.29, pidcut = E_probe_PID_E > 2

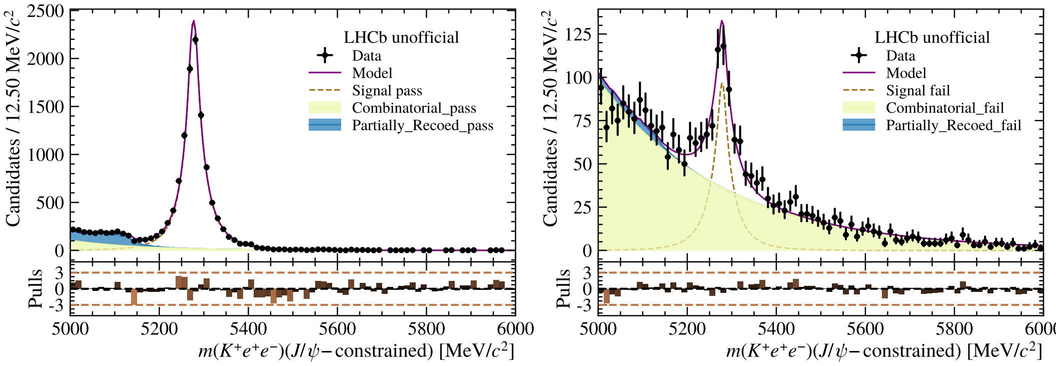

Fig. 25: Fit inbinx-axis-idx=2,y-axis-idx=1

Bin (2,2): E_probe_PT>= 2500.0 && E_probe_PT < 4000.0 & E_probe_ETA>= 3.1 && E_probe_ETA < 3.8 cut with efficiency 95.56+/-0.32, pidcut = E_probe_PID_E > 2

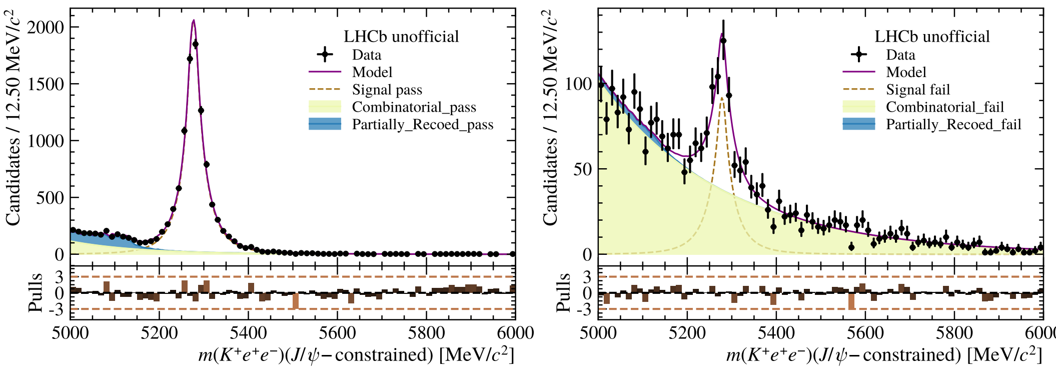

Fig. 26: Fit inbinx-axis-idx=2,y-axis-idx=2

Bin (2,3): E_probe_PT>= 2500.0 && E_probe_PT < 4000.0 & E_probe_ETA>= 3.8 && E_probe_ETA < 5.2 cut with efficiency 93.87+/-0.79, pidcut = E_probe_PID_E > 2

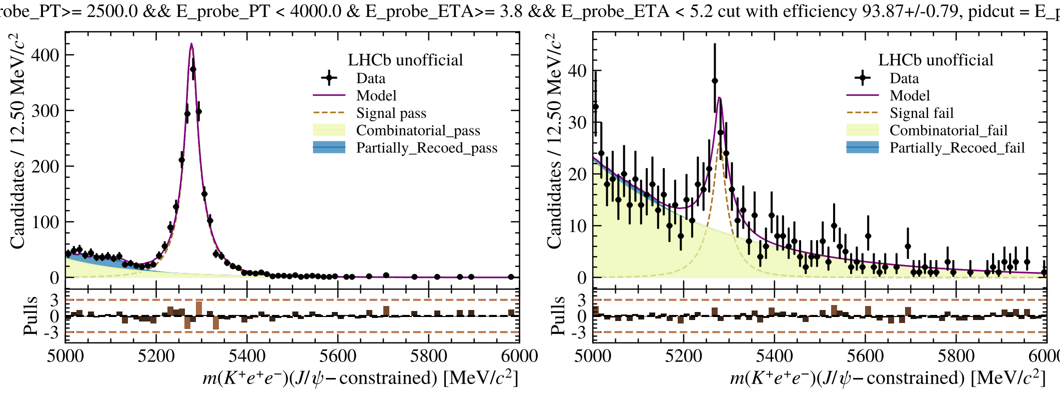

Fig. 27: Fit inbinx-axis-idx=2,y-axis-idx=3

Bin (3,0): E_probe_PT>= 4000.0 && E_probe_PT < 9000.0 & E_probe_ETA>= 1.5 && E_probe_ETA < 2.5 cut with efficiency 96.08+/-0.39, pidcut = E_probe_PID_E > 2

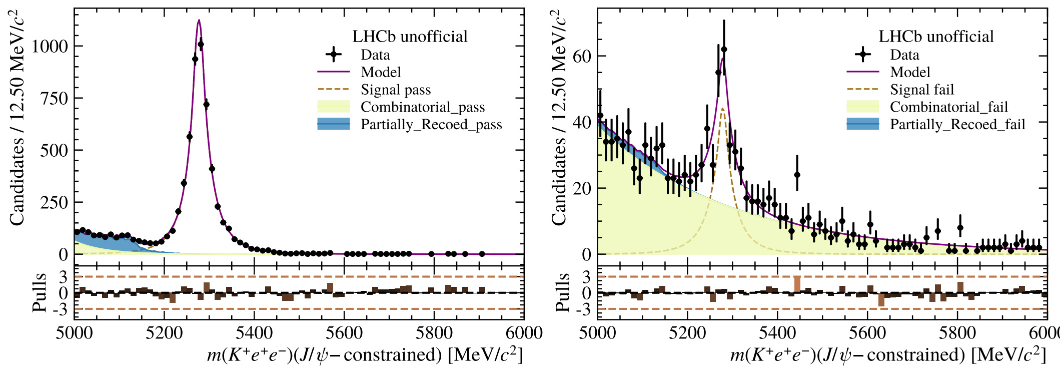

Fig. 28: Fit inbinx-axis-idx=3,y-axis-idx=0

Bin (3,1): E_probe_PT>= 4000.0 && E_probe_PT < 9000.0 & E_probe_ETA>= 2.5 && E_probe_ETA < 3.1 cut with efficiency 96.02+/-0.28, pidcut = E_probe_PID_E > 2

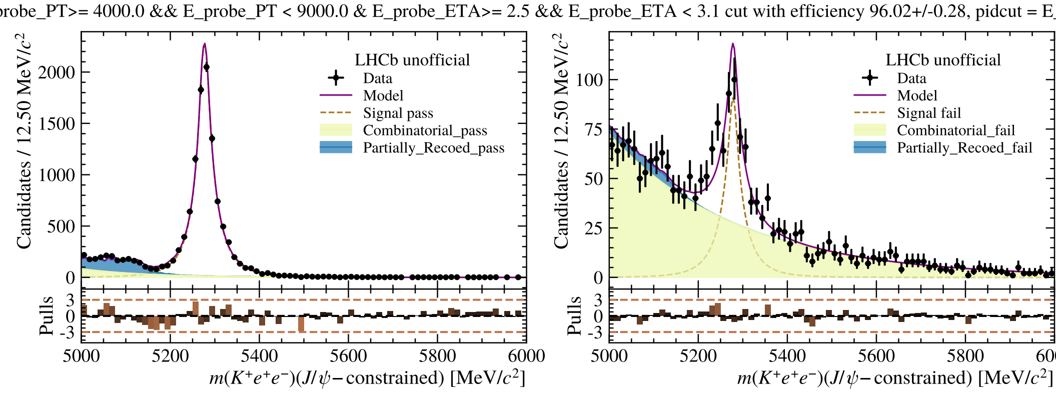

Fig. 29: Fit inbinx-axis-idx=3,y-axis-idx=1

Bin (3,2): E_probe_PT>= 4000.0 && E_probe_PT < 9000.0 & E_probe_ETA>= 3.1 && E_probe_ETA < 3.8 cut with efficiency 96.56+/-0.31, pidcut = E_probe_PID_E > 2

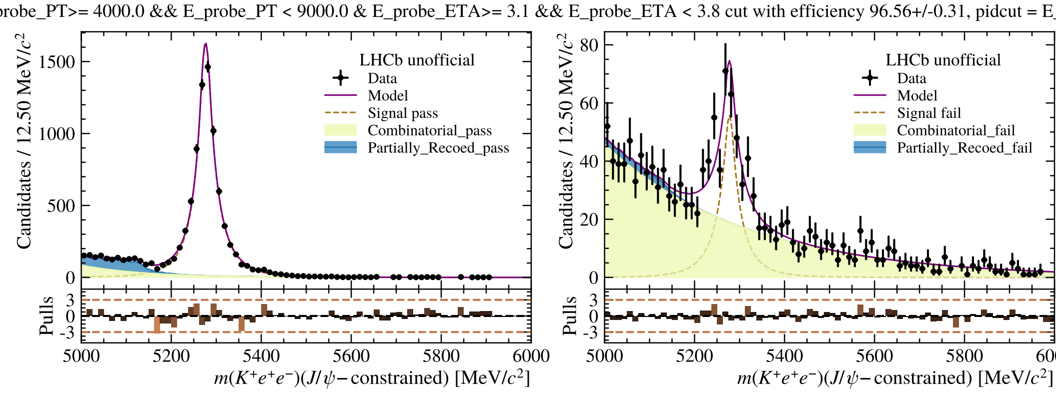

Fig. 30: Fit inbinx-axis-idx=3,y-axis-idx=2

Bin (3,3): E_probe_PT>= 4000.0 && E_probe_PT < 9000.0 & E_probe_ETA>= 3.8 && E_probe_ETA < 5.2 cut with efficiency 94.43+/-1.06, pidcut = E_probe_PID_E > 2

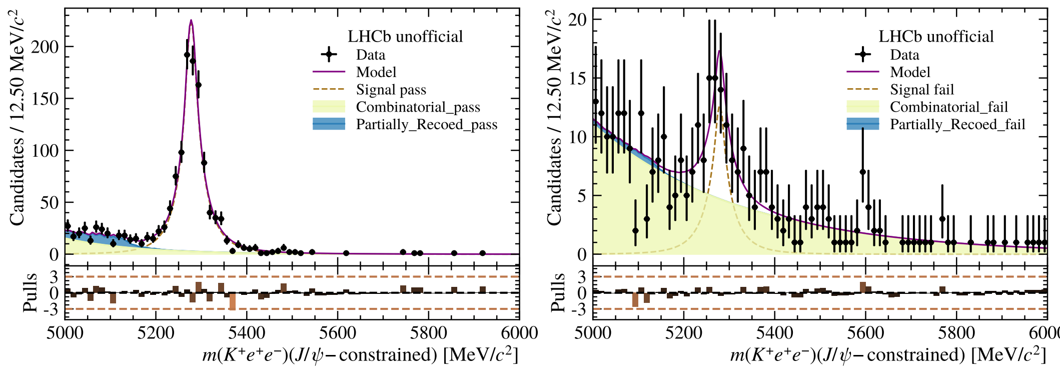

Fig. 31: Fit inbinx-axis-idx=3,y-axis-idx=3

Bin (4,0): E_probe_PT>= 9000.0 && E_probe_PT < 25000.0 & E_probe_ETA>= 1.5 && E_probe_ETA < 2.5 cut with efficiency 96.19+/-0.85, pidcut = E_probe_PID_E > 2

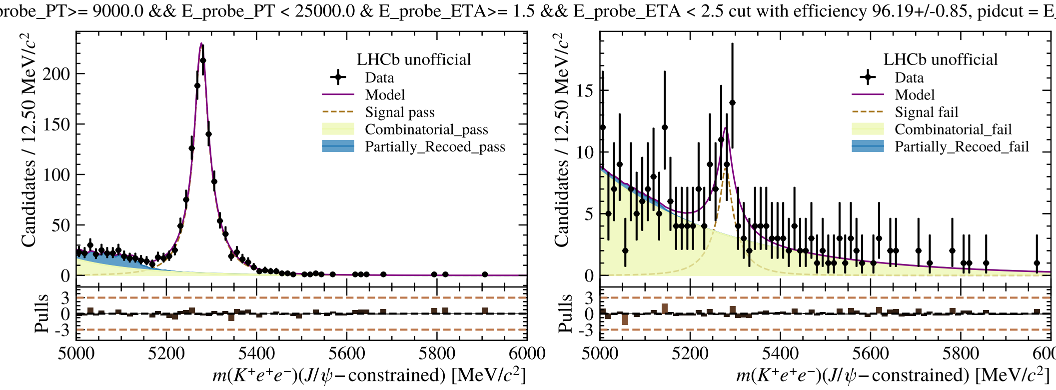

Fig. 32: Fit inbinx-axis-idx=4,y-axis-idx=0

Bin (4,1): E_probe_PT>= 9000.0 && E_probe_PT < 25000.0 & E_probe_ETA>= 2.5 && E_probe_ETA < 3.1 cut with efficiency 94.44+/-0.78, pidcut = E_probe_PID_E > 2

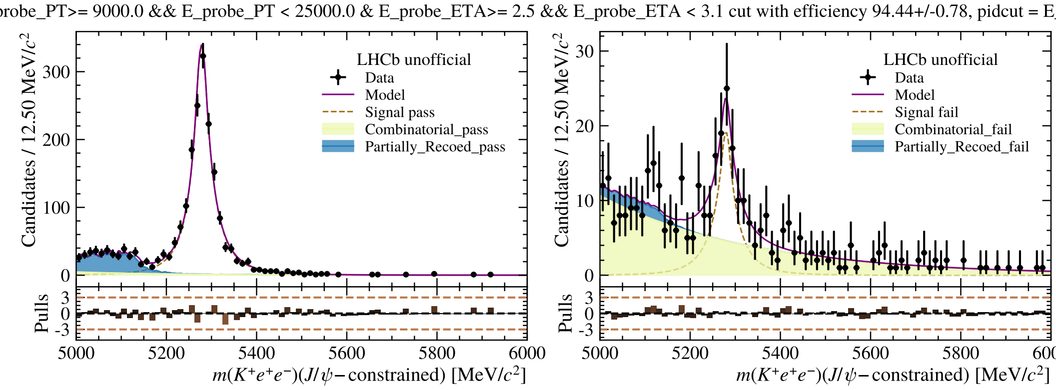

Fig. 33: Fit inbinx-axis-idx=4,y-axis-idx=1

9 Appendix B

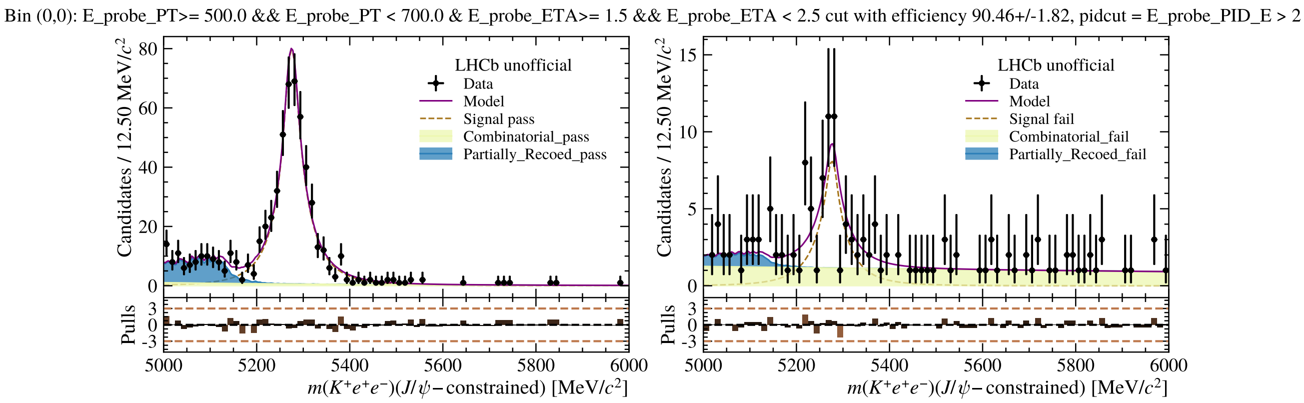

Fig. 34: Fit inbinx-axis-idx=0,y-axis-idx=0

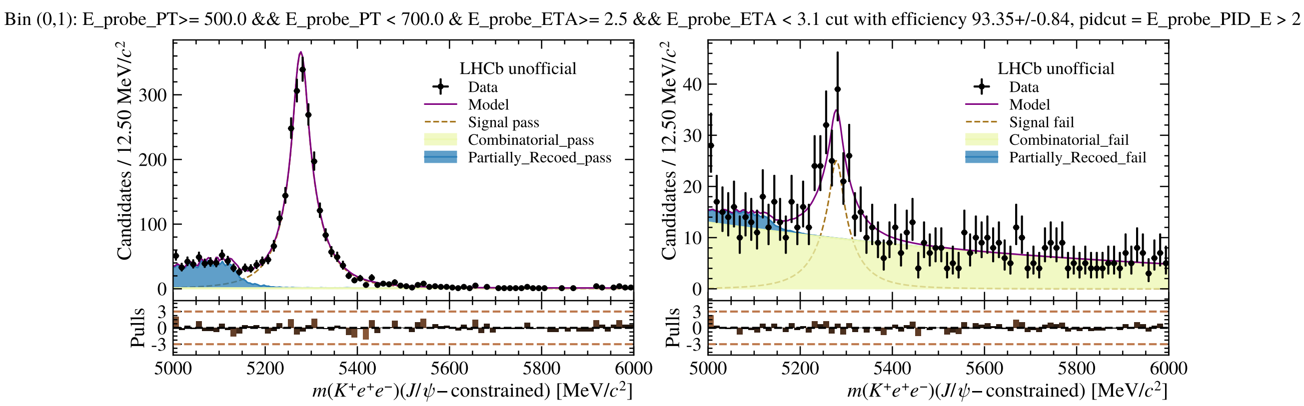

Fig. 35: Fit inbinx-axis-idx=0,y-axis-idx=1

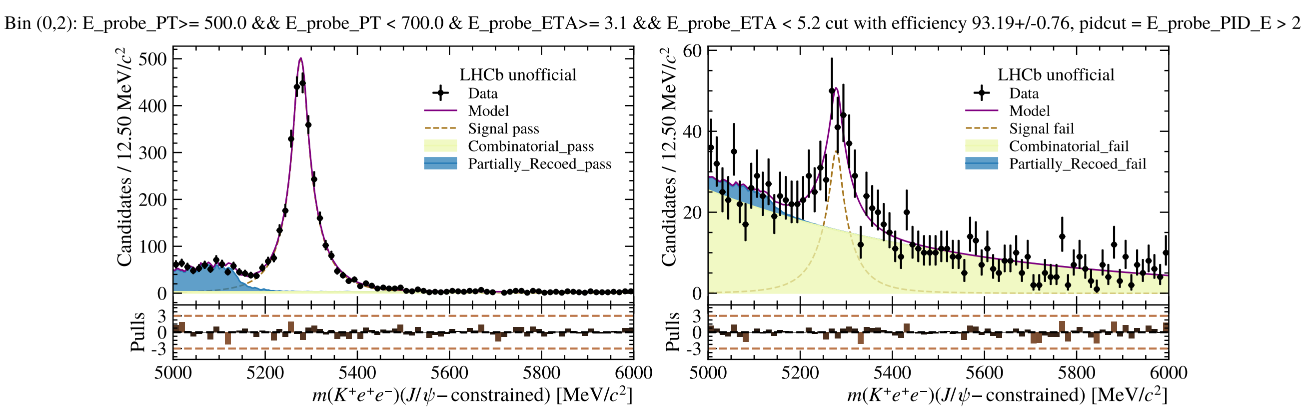

Fig. 36: Fit inbinx-axis-idx=0,y-axis-idx=2

Bin (1,0): E_probe_PT>= 700.0 && E_probe_PT < 2500.0 & E_probe_ETA>= 1.5 && E_probe_ETA < 2.5 cut with efficiency 98.14+/-0.18, pidcut = E_probe_PID_E > 2

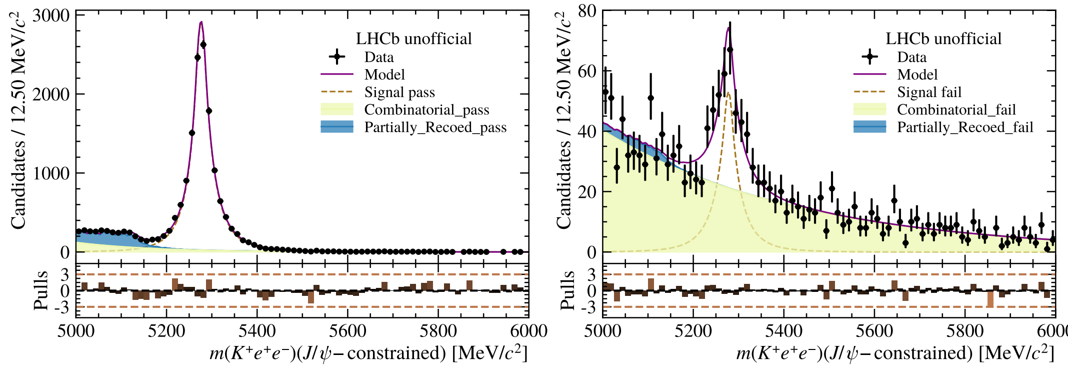

Fig. 37: Fit inbinx-axis-idx=1,y-axis-idx=0

Bin (1,1): E_probe_PT>= 700.0 && E_probe_PT < 2500.0 & E_probe_ETA>= 2.5 && E_probe_ETA < 3.1 cut with efficiency 96.46+/-0.18, pidcut = E_probe_PID_E > 2

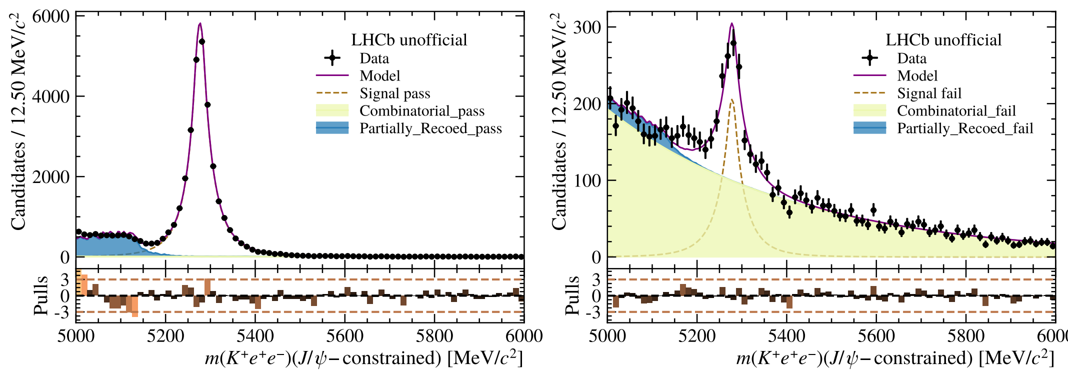

Fig. 38: Fit inbinx-axis-idx=1,y-axis-idx=1

Bin (1,2): E_probe_PT>= 700.0 && E_probe_PT < 2500.0 & E_probe_ETA>= 3.1 && E_probe_ETA < 5.2 cut with efficiency 93.00+/-0.22, pidcut = E_probe_PID_E > 2

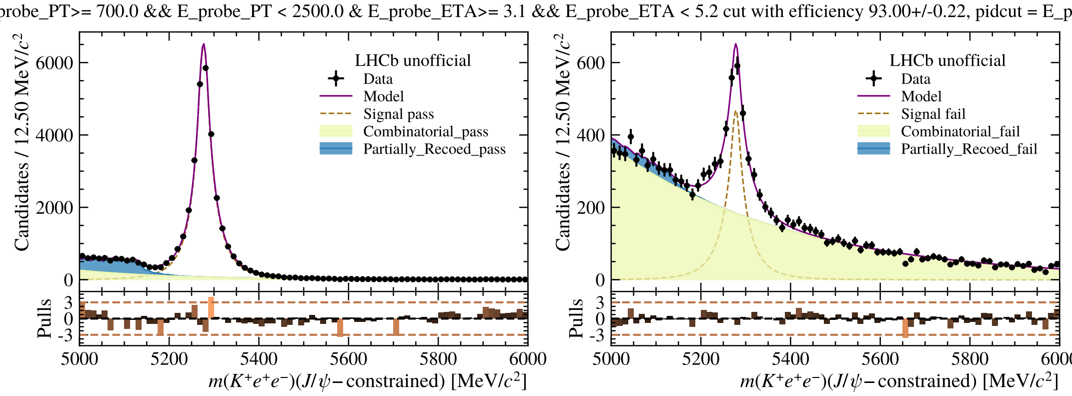

Fig. 39: Fit inbinx-axis-idx=1,y-axis-idx=2

Bin (2,0): E_probe_PT>= 2500.0 && E_probe_PT < 4000.0 & E_probe_ETA>= 1.5 && E_probe_ETA < 2.5 cut with efficiency 97.47+/-0.33, pidcut = E_probe_PID_E > 2

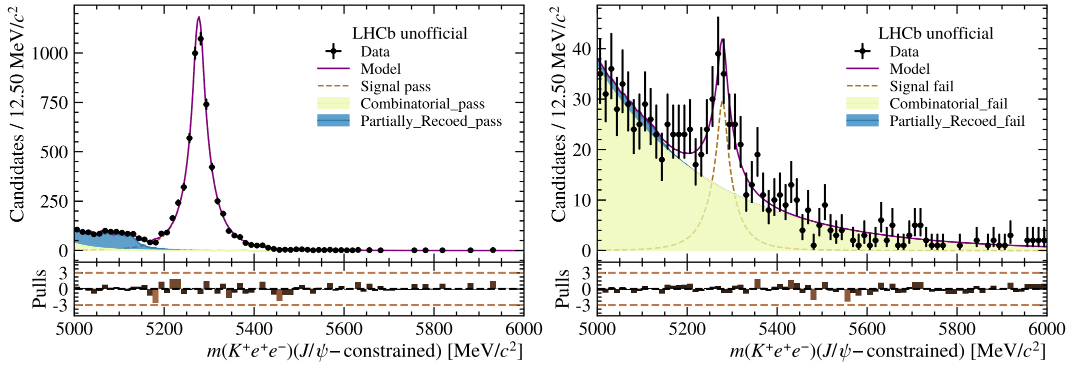

Fig. 40: Fit inbinx-axis-idx=2,y-axis-idx=0

Bin (2,1): E_probe_PT>= 2500.0 && E_probe_PT < 4000.0 & E_probe_ETA>= 2.5 && E_probe_ETA < 3.1 cut with efficiency 95.97+/-0.28, pidcut = E_probe_PID_E > 2

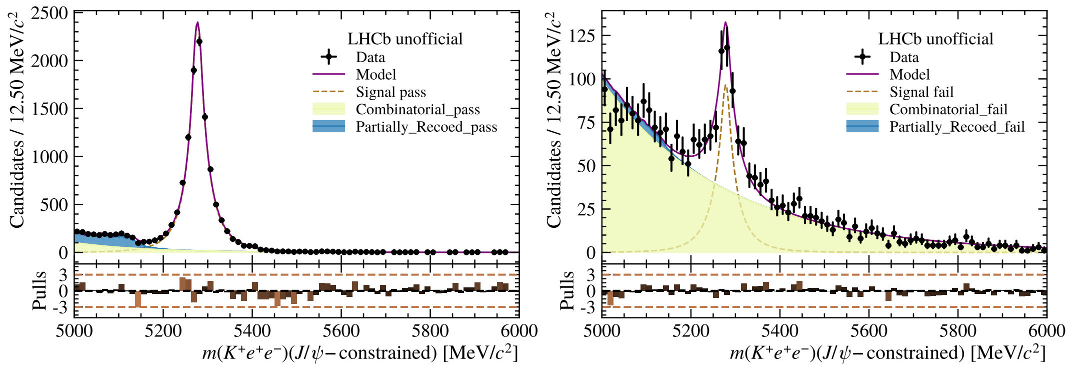

Fig. 41: Fit inbinx-axis-idx=2,y-axis-idx=1

Bin (2,2): E_probe_PT>= 2500.0 && E_probe_PT < 4000.0 & E_probe_ETA>= 3.1 && E_probe_ETA < 5.2 cut with efficiency 95.57+/-0.32, pidcut = E_probe_PID_E > 2

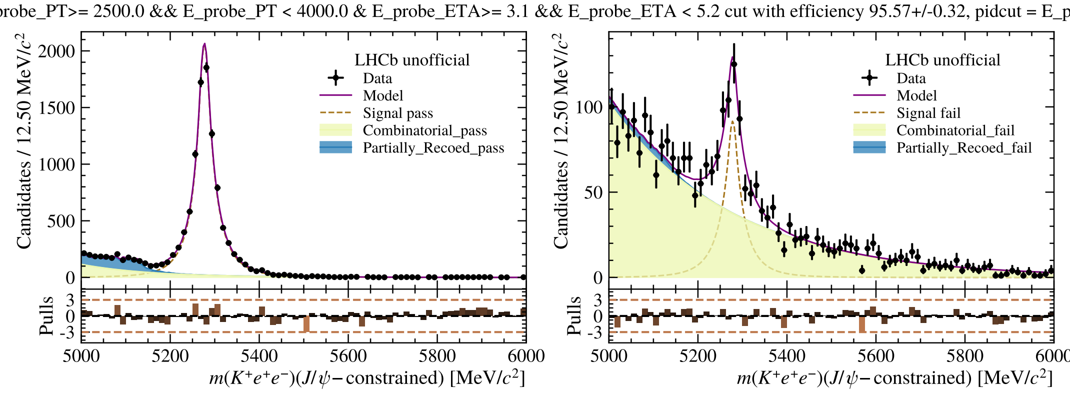

Fig. 42: Fit inbinx-axis-idx=2,y-axis-idx=2

Bin (3,0): E_probe_PT>= 4000.0 && E_probe_PT < 9000.0 & E_probe_ETA>= 1.5 && E_probe_ETA < 2.5 cut with efficiency 96.10+/-0.39, pidcut = E_probe_PID_E > 2

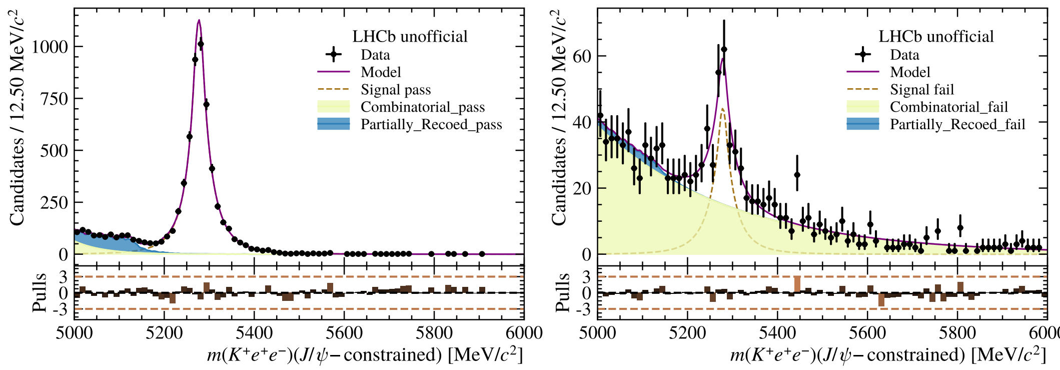

Fig. 43: Fit inbinx-axis-idx=3,y-axis-idx=0

Bin (3,1): E_probe_PT>= 4000.0 && E_probe_PT < 9000.0 & E_probe_ETA>= 2.5 && E_probe_ETA < 3.1 cut with efficiency 96.02+/-0.28, pidcut = E_probe_PID_E > 2

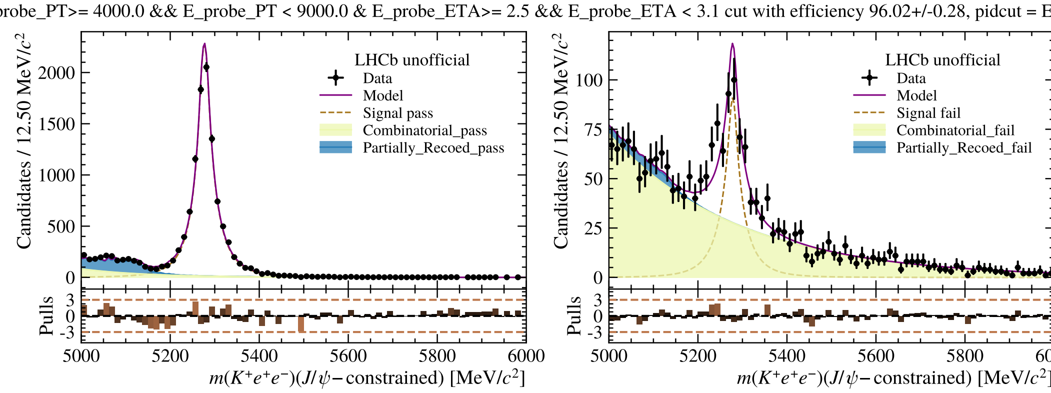

Fig. 44: Fit inbinx-axis-idx=3,y-axis-idx=1

Bin (3,2): E_probe_PT>= 4000.0 && E_probe_PT < 9000.0 & E_probe_ETA>= 3.1 && E_probe_ETA < 5.2 cut with efficiency 96.56+/-0.31, pidcut = E_probe_PID_E > 2

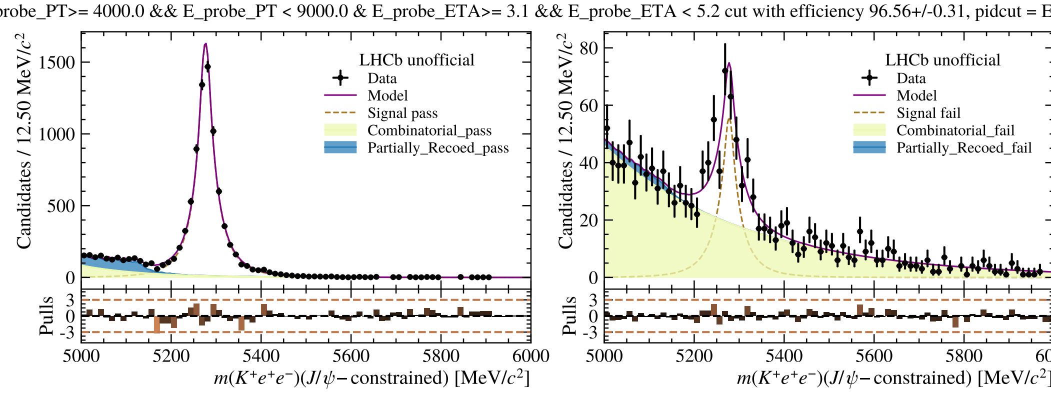

Fig. 45: Fit inbinx-axis-idx=3,y-axis-idx=2

Bin (4,0): E_probe_PT>= 9000.0 && E_probe_PT < 25000.0 & E_probe_ETA>= 1.5 && E_probe_ETA < 2.5 cut with efficiency 96.18+/-0.85, pidcut = E_probe_PID_E > 2

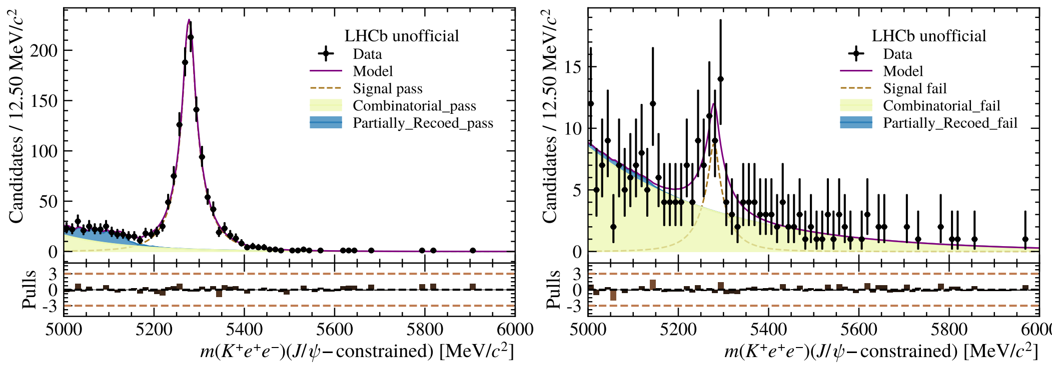

Fig. 46: Fit inbinx-axis-idx=4,y-axis-idx=0

Bin (4,1): E_probe_PT>= 9000.0 && E_probe_PT < 25000.0 & E_probe_ETA>= 2.5 && E_probe_ETA < 3.1 cut with efficiency 94.45+/-0.78, pidcut = E_probe_PID_E > 2

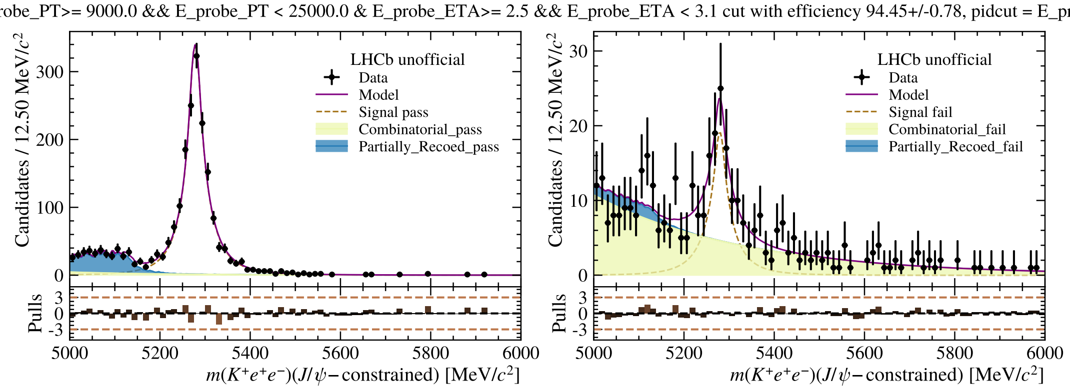

Fig. 47: Fit inbinx-axis-idx=4,y-axis-idx=1

Bin (4,2): E_probe_PT>= 9000.0 && E_probe_PT < 25000.0 & E_probe_ETA>= 3.1 && E_probe_ETA < 5.2 cut with efficiency 96.80+/-0.90, pidcut = E_probe_PID_E > 2

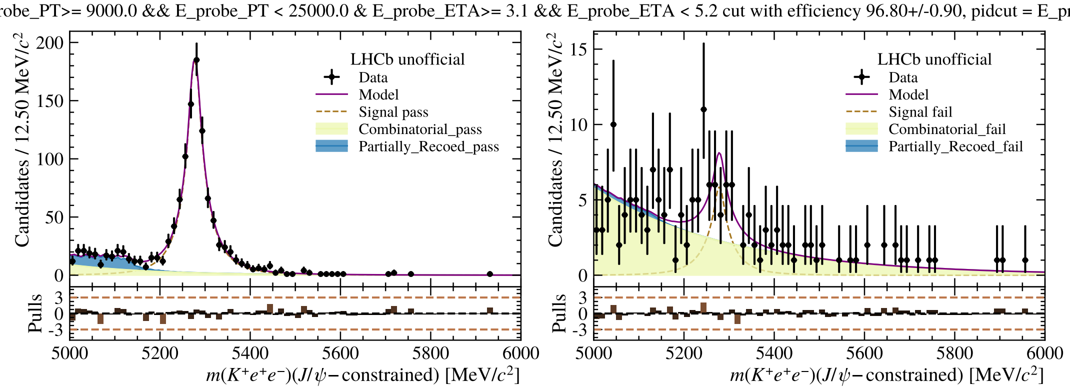

Fig. 48: Fit inbinx-axis-idx=4,y-axis-idx=2

10 Appendix C

Bin (0,0): E_probe_PT>= 500.0 && E_probe_PT < 700.0 & E_probe_ETA>= 1.5 && E_probe_ETA < 2.5 cut with efficiency 92.29+/-3.61, pidcut = E_probe_PID_E > 0

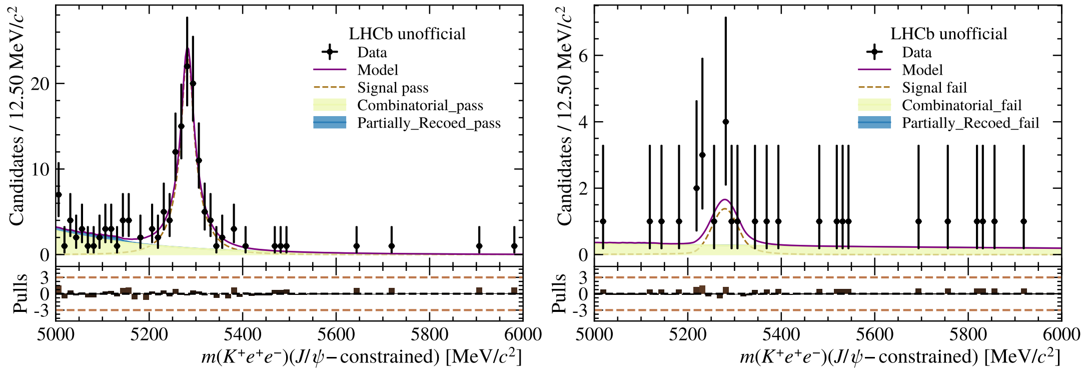

Fig. 49: Fit inbinx-axis-idx=0,y-axis-idx=0

Bin (0,1): E_probe_PT>= 500.0 && E_probe_PT < 700.0 & E_probe_ETA>= 2.5 && E_probe_ETA < 3.1 cut with efficiency 95.40+/-1.16, pidcut = E_probe_PID_E > 0

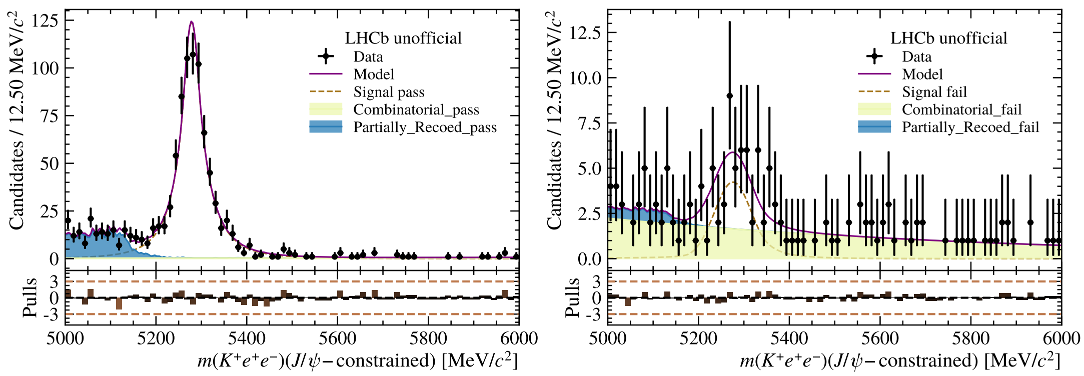

Fig. 50: Fit inbinx-axis-idx=0,y-axis-idx=1

Bin (0,2): E_probe_PT>= 500.0 && E_probe_PT < 700.0 & E_probe_ETA>= 3.1 && E_probe_ETA < 5.2 cut with efficiency 97.03+/-0.79, pidcut = E_probe_PID_E > 0

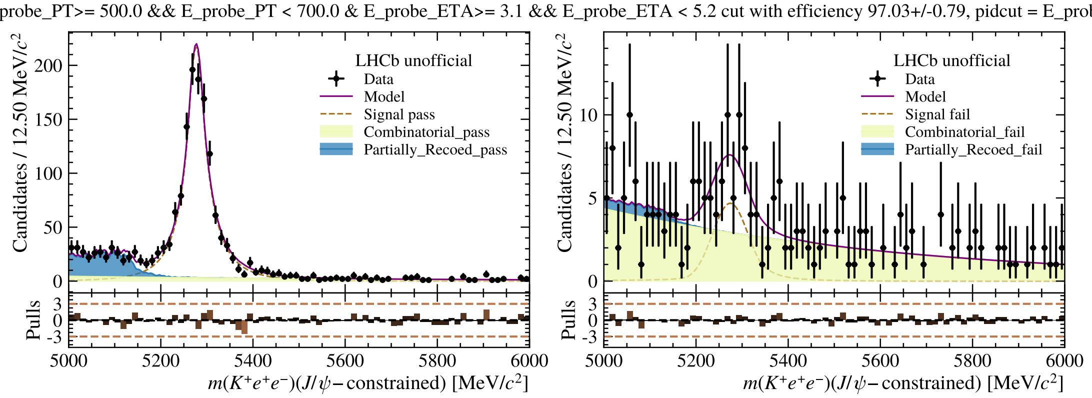

Fig. 51: Fit inbinx-axis-idx=0,y-axis-idx=2

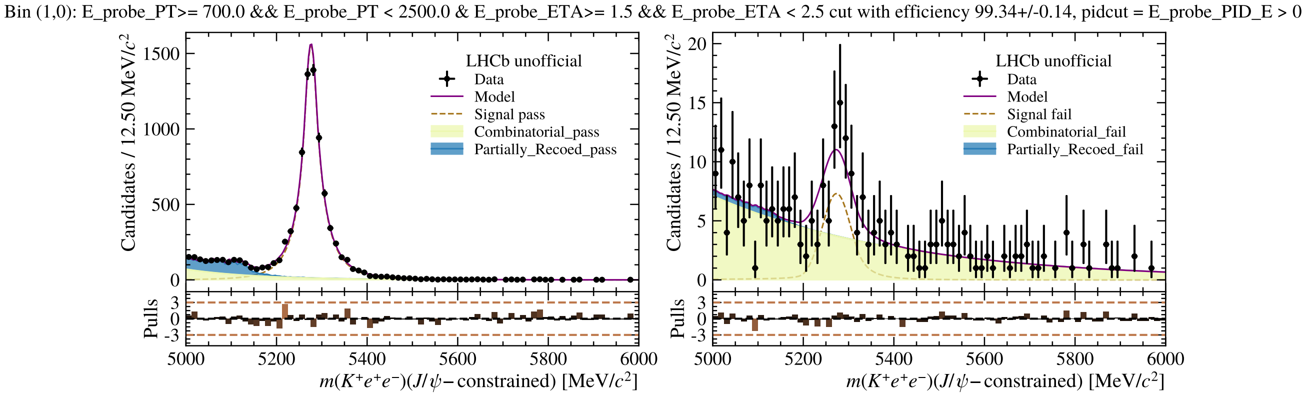

Fig. 52: Fit inbinx-axis-idx=1,y-axis-idx=0

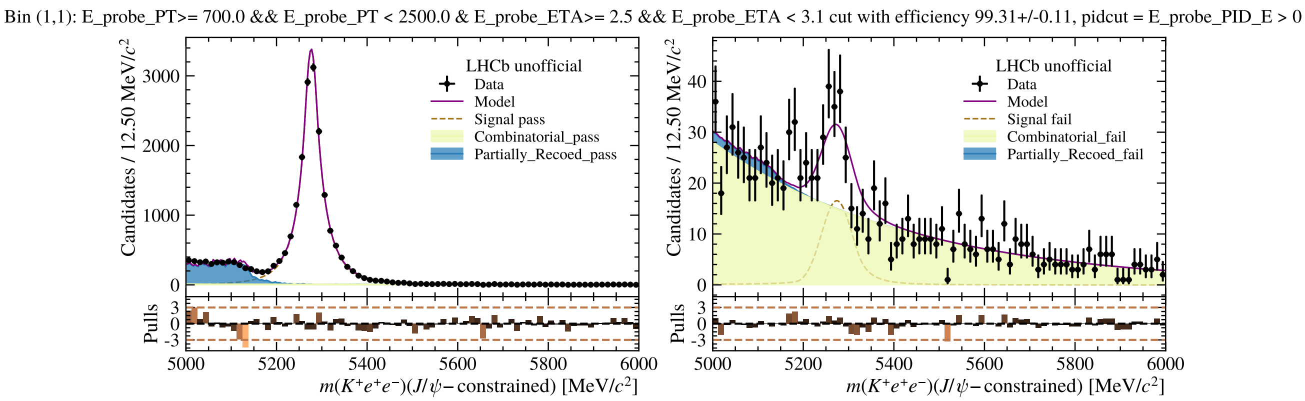

Fig. 53: Fit inbinx-axis-idx=1,y-axis-idx=1

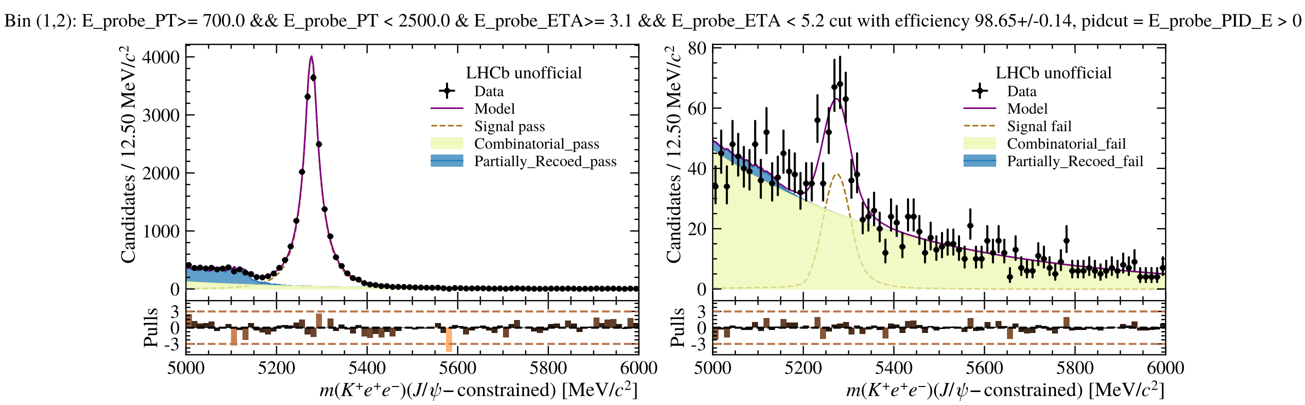

Fig. 54: Fit inbinx-axis-idx=1,y-axis-idx=2

Bin (2,0): E_probe_PT>= 2500.0 && E_probe_PT < 4000.0 & E_probe_ETA>= 1.5 && E_probe_ETA < 2.5 cut with efficiency 99.86+/-0.13, pidcut = E_probe_PID_E > 0

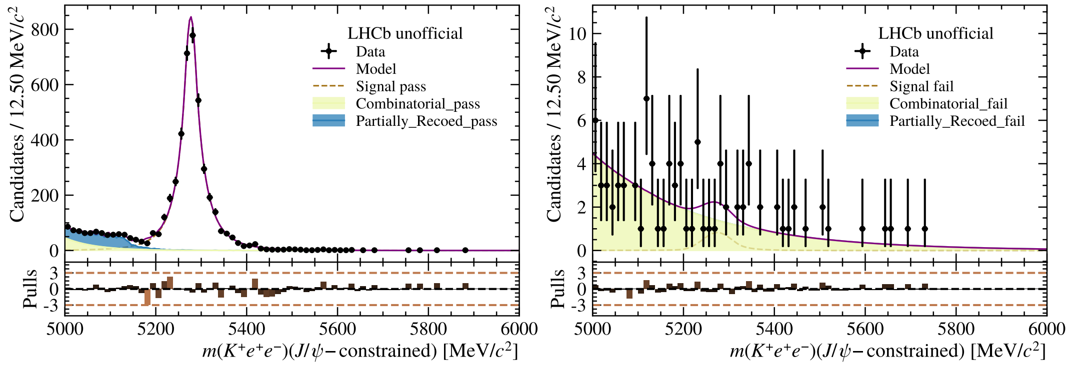

Fig. 55: Fit inbinx-axis-idx=2,y-axis-idx=0

Bin (2,1): E_probe_PT>= 2500.0 && E_probe_PT < 4000.0 & E_probe_ETA>= 2.5 && E_probe_ETA < 3.1 cut with efficiency 99.26+/-0.14, pidcut = E_probe_PID_E > 0

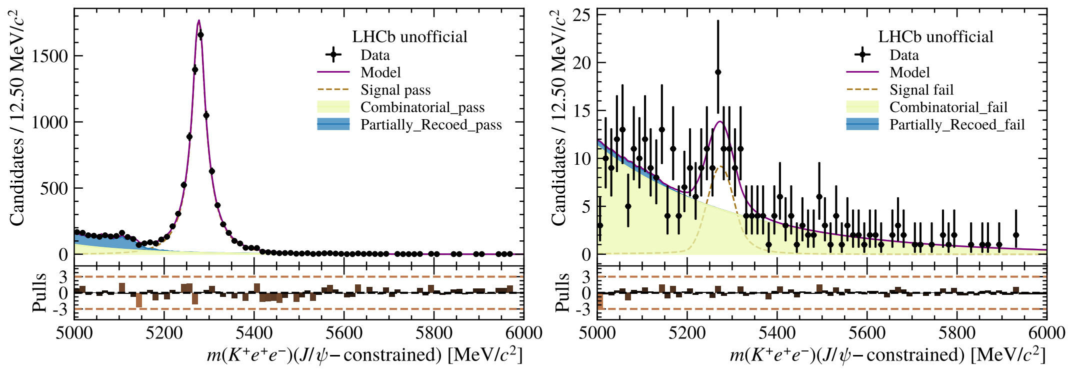

Fig. 56: Fit inbinx-axis-idx=2,y-axis-idx=1

Bin (2,2): E_probe_PT>= 2500.0 && E_probe_PT < 4000.0 & E_probe_ETA>= 3.1 && E_probe_ETA < 5.2 cut with efficiency 99.04+/-0.17, pidcut = E_probe_PID_E > 0

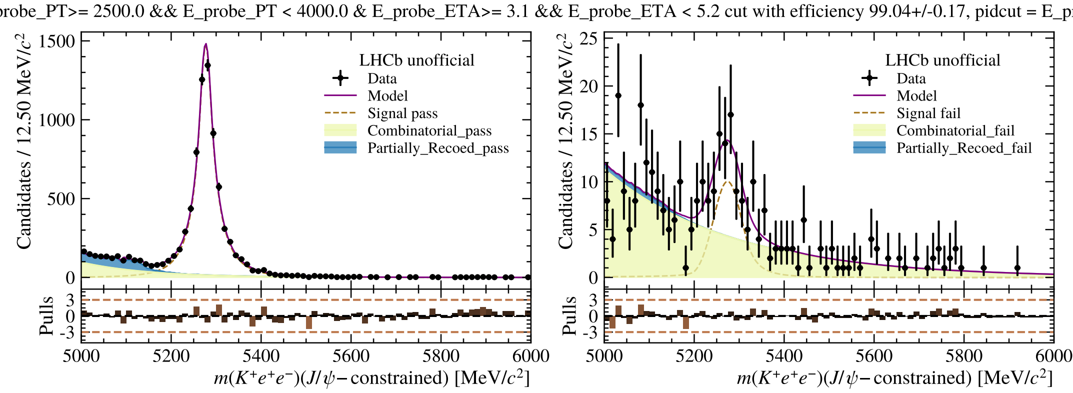

Fig. 57: Fit inbinx-axis-idx=2,y-axis-idx=2

Bin (3,0): E_probe_PT>= 4000.0 && E_probe_PT < 9000.0 & E_probe_ETA>= 1.5 && E_probe_ETA < 2.5 cut with efficiency 99.48+/-0.18, pidcut = E_probe_PID_E > 0

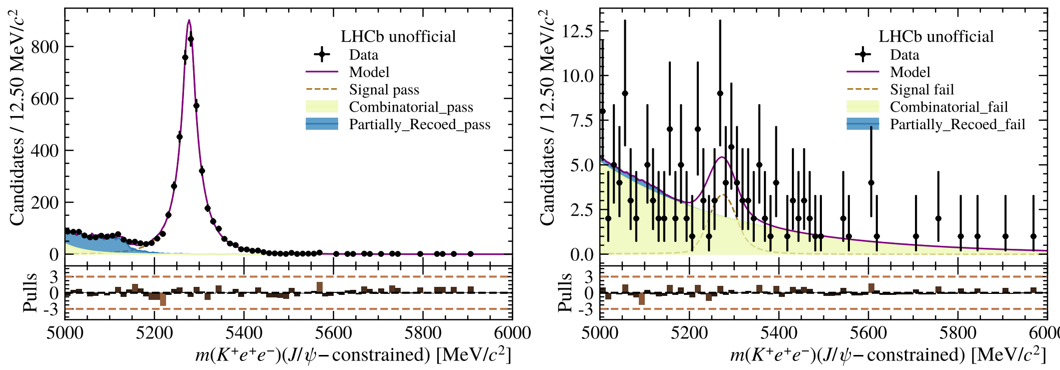

Fig. 58: Fit inbinx-axis-idx=3,y-axis-idx=0

Bin (3,1): E_probe_PT>= 4000.0 && E_probe_PT < 9000.0 & E_probe_ETA>= 2.5 && E_probe_ETA < 3.1 cut with efficiency 99.14+/-0.15, pidcut = E_probe_PID_E > 0

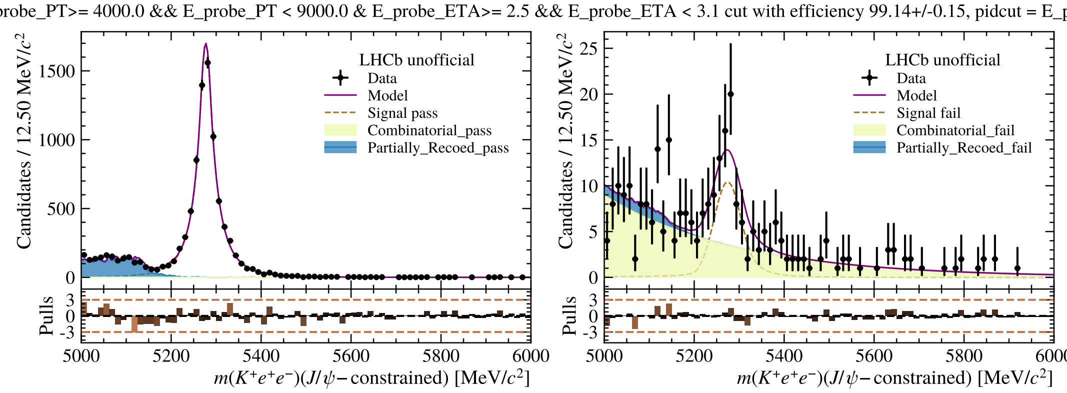

Fig. 59: Fit inbinx-axis-idx=3,y-axis-idx=1

Bin (3,2): E_probe_PT>= 4000.0 && E_probe_PT < 9000.0 & E_probe_ETA>= 3.1 && E_probe_ETA < 5.2 cut with efficiency 99.17+/-0.16, pidcut = E_probe_PID_E > 0

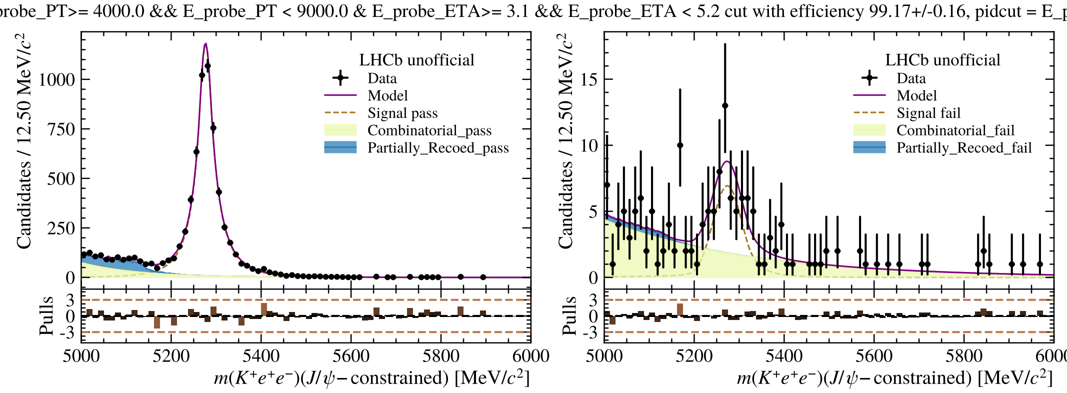

Fig. 60: Fit inbinx-axis-idx=3,y-axis-idx=2

Bin (4,0): E_probe_PT>= 9000.0 && E_probe_PT < 25000.0 & E_probe_ETA>= 1.5 && E_probe_ETA < 2.5 cut with efficiency 99.59+/-0.33, pidcut = E_probe_PID_E > 0

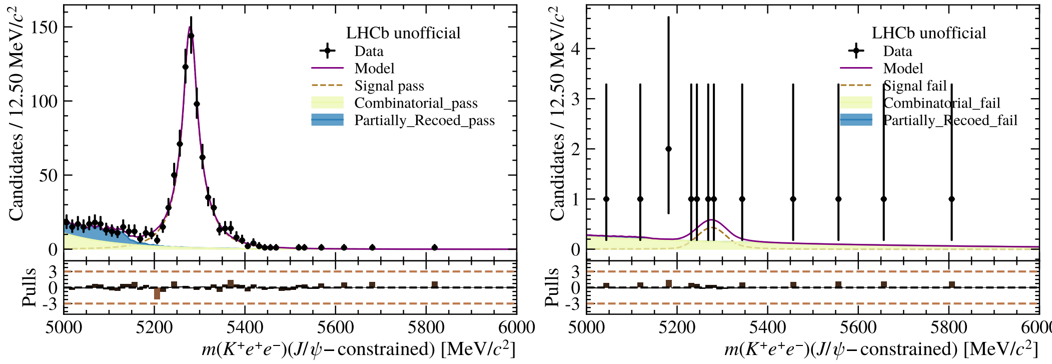

Fig. 61: Fit inbinx-axis-idx=4,y-axis-idx=0

Bin (4,1): E_probe_PT>= 9000.0 && E_probe_PT < 25000.0 & E_probe_ETA>= 2.5 && E_probe_ETA < 3.1 cut with efficiency 98.57+/-0.47, pidcut = E_probe_PID_E > 0

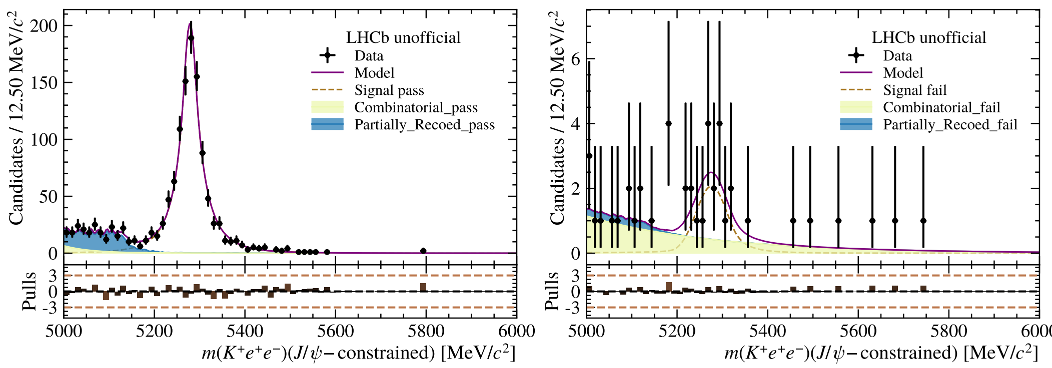

Fig. 62: Fit inbinx-axis-idx=4,y-axis-idx=1

Bin (4,2): E_probe_PT>= 9000.0 && E_probe_PT < 25000.0 & E_probe_ETA>= 3.1 && E_probe_ETA < 5.2 cut with efficiency 98.84+/-0.64, pidcut = E_probe_PID_E > 0

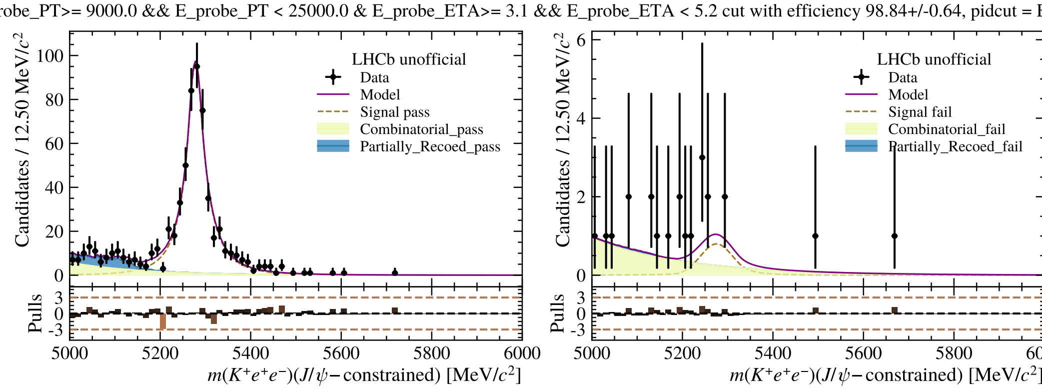

Fig. 63: Fit inbinx-axis-idx=4,y-axis-idx=2

11 Appendix D

Bin (0,0): E_probe_PT>= 500.0 && E_probe_PT < 700.0 & E_probe_ETA>= 1.5 && E_probe_ETA < 2.5 cut with efficiency 91.07+/-4.42, pidcut = E_probe_PID_E > 1.5

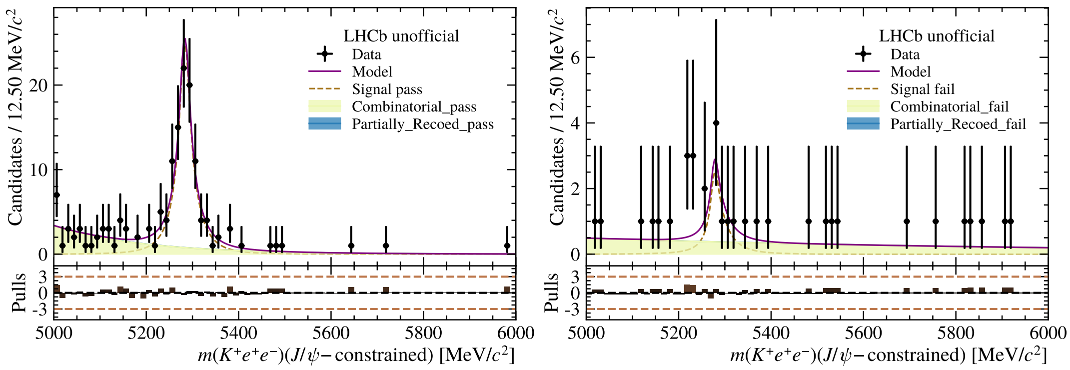

Fig. 64: Fit inbinx-axis-idx=0,y-axis-idx=0

Bin (0,1): E_probe_PT>= 500.0 && E_probe_PT < 700.0 & E_probe_ETA>= 2.5 && E_probe_ETA < 3.1 cut with efficiency 92.89+/-1.32, pidcut = E_probe_PID_E > 1.5

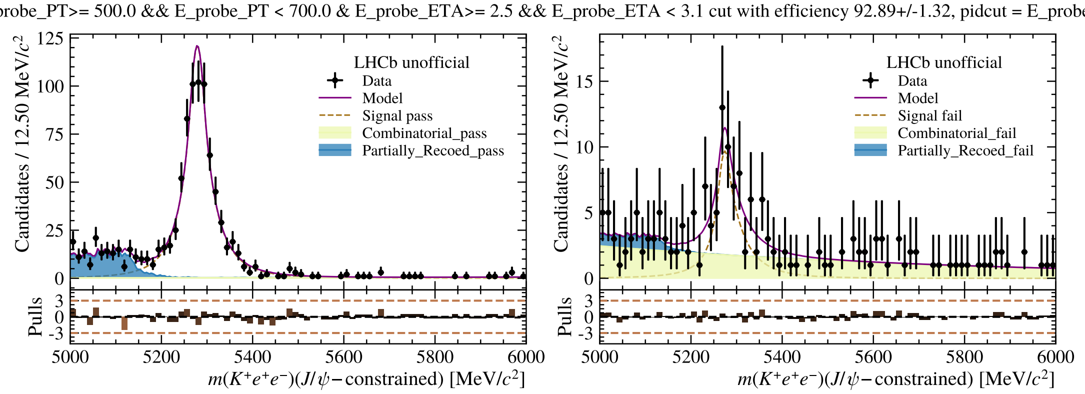

Fig. 65: Fit inbinx-axis-idx=0,y-axis-idx=1

Bin (0,2): E_probe_PT>= 500.0 && E_probe_PT < 700.0 & E_probe_ETA>= 3.1 && E_probe_ETA < 5.2 cut with efficiency 95.54+/-0.89, pidcut = E_probe_PID_E > 1.5

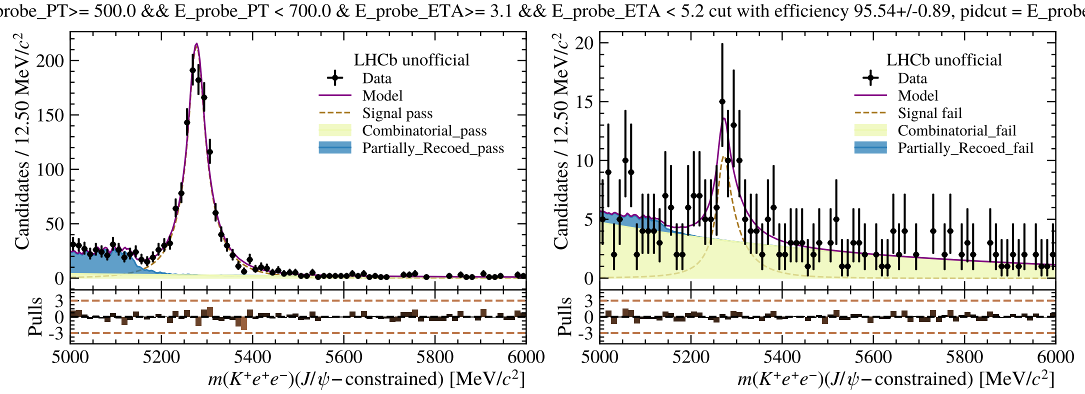

Fig. 66: Fit inbinx-axis-idx=0,y-axis-idx=2

Bin (1,0): E_probe_PT>= 700.0 && E_probe_PT < 2500.0 & E_probe_ETA>= 1.5 && E_probe_ETA < 2.5 cut with efficiency 98.65+/-0.18, pidcut = E_probe_PID_E > 1.5

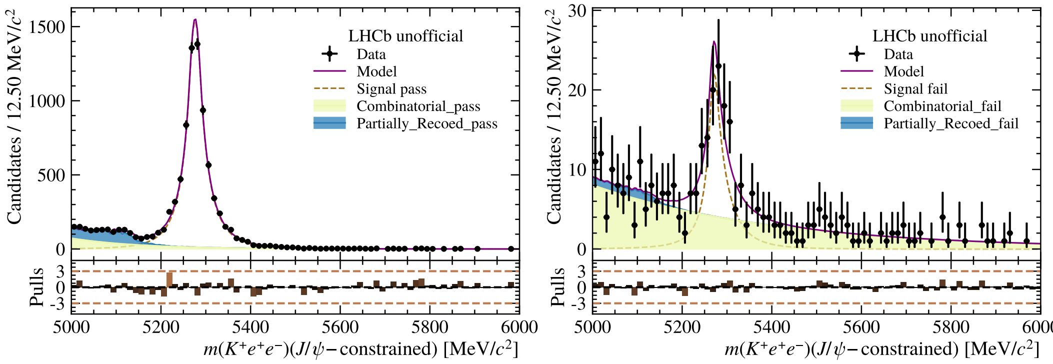

Fig. 67: Fit inbinx-axis-idx=1,y-axis-idx=0

Bin (1,1): E_probe_PT>= 700.0 && E_probe_PT < 2500.0 & E_probe_ETA>= 2.5 && E_probe_ETA < 3.1 cut with efficiency 98.76+/-0.13, pidcut = E_probe_PID_E > 1.5

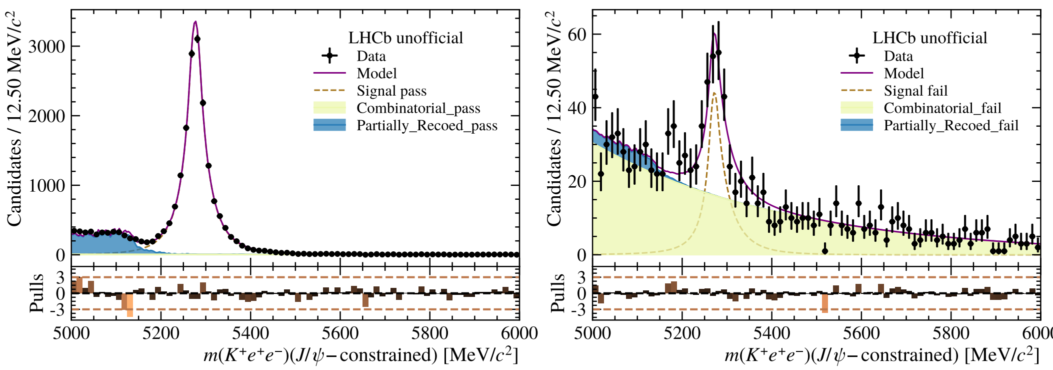

Fig. 68: Fit inbinx-axis-idx=1,y-axis-idx=1

Bin (1,2): E_probe_PT>= 700.0 && E_probe_PT < 2500.0 & E_probe_ETA>= 3.1 && E_probe_ETA < 5.2 cut with efficiency 97.43+/-0.17, pidcut = E_probe_PID_E > 1.5

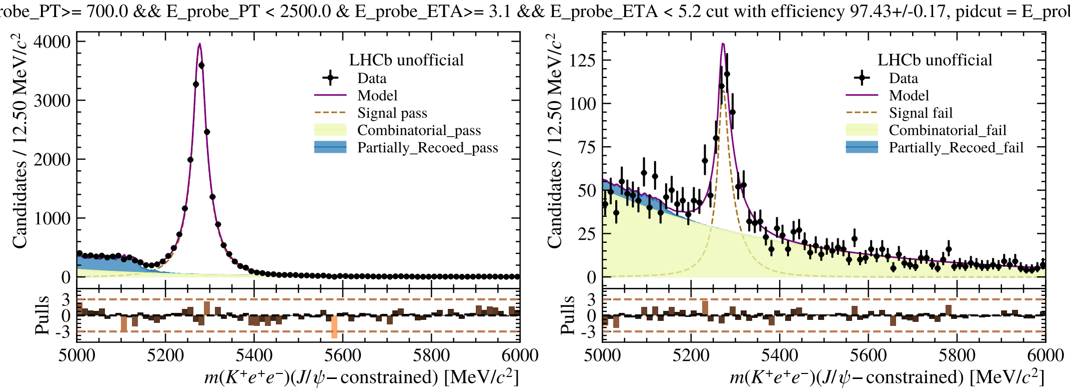

Fig. 69: Fit inbinx-axis-idx=1,y-axis-idx=2

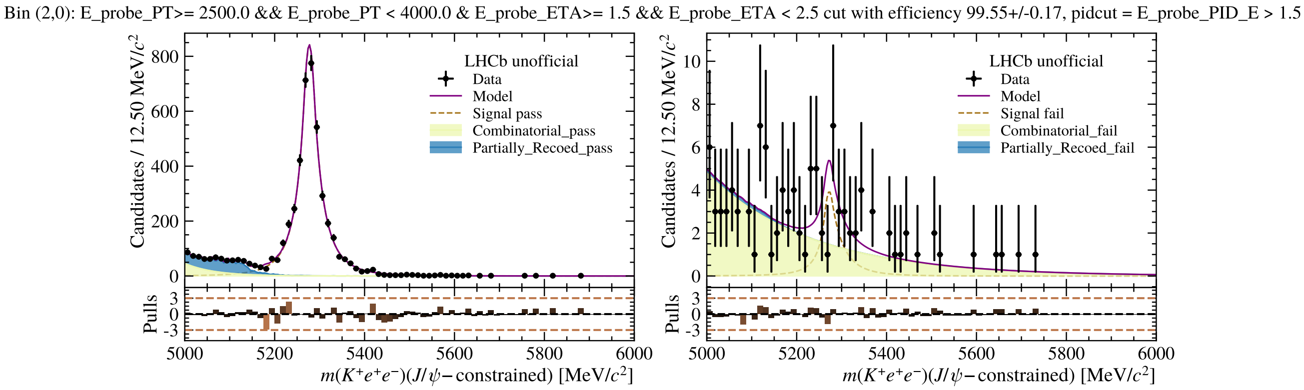

Fig. 70: Fit inbinx-axis-idx=2,y-axis-idx=0

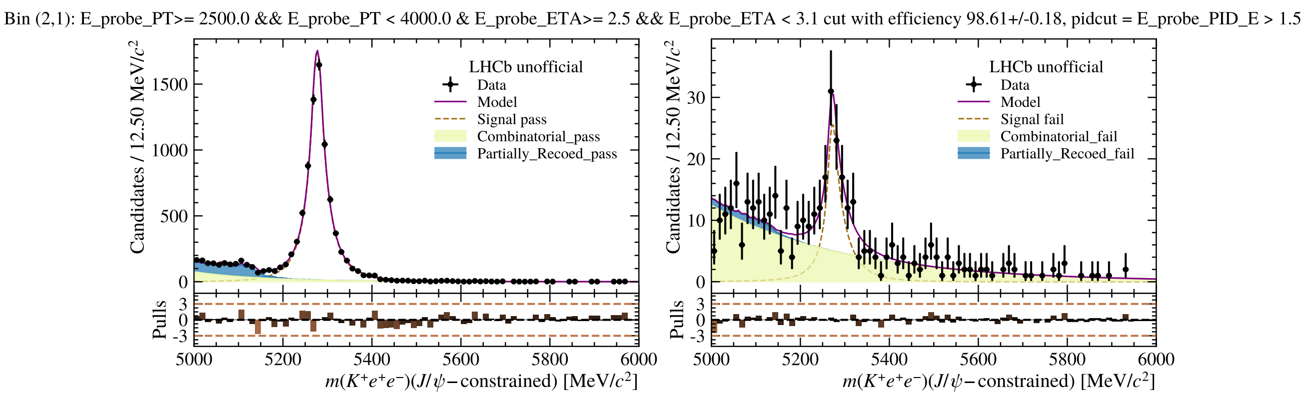

Fig. 71: Fit inbinx-axis-idx=2,y-axis-idx=1

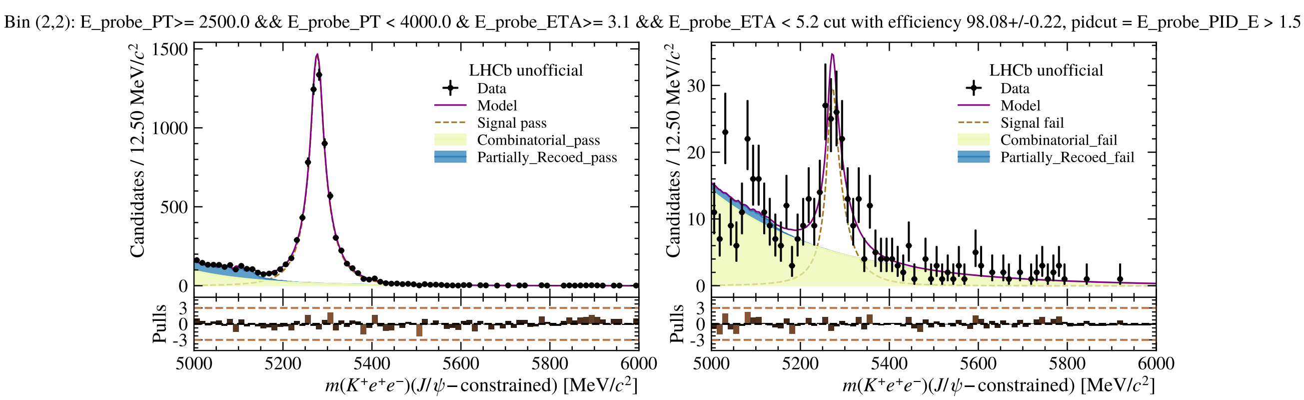

Fig. 72: Fit inbinx-axis-idx=2,y-axis-idx=2

Bin (3,0): E_probe_PT>= 4000.0 && E_probe_PT < 9000.0 & E_probe_ETA>= 1.5 && E_probe_ETA < 2.5 cut with efficiency 98.91+/-0.22, pidcut = E_probe_PID_E > 1.5

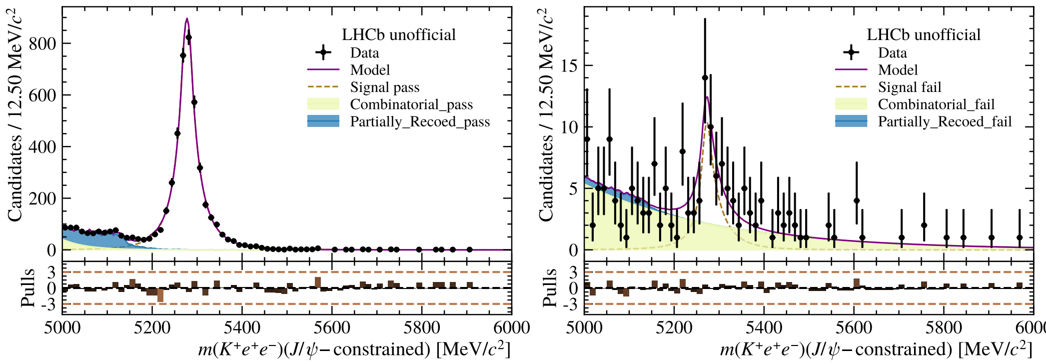

Fig. 73: Fit inbinx-axis-idx=3,y-axis-idx=0

Bin (3,1): E_probe_PT>= 4000.0 && E_probe_PT < 9000.0 & E_probe_ETA>= 2.5 && E_probe_ETA < 3.1 cut with efficiency 98.15+/-0.20, pidcut = E_probe_PID_E > 1.5

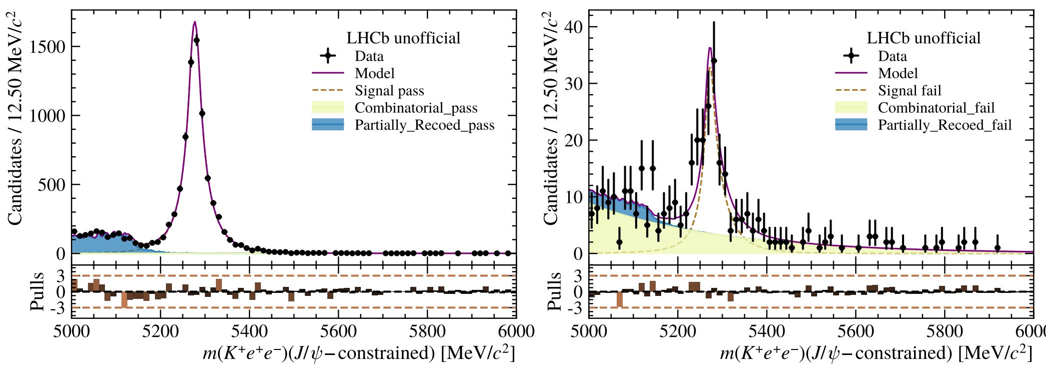

Fig. 74: Fit inbinx-axis-idx=3,y-axis-idx=1

Bin (3,2): E_probe_PT>= 4000.0 && E_probe_PT < 9000.0 & E_probe_ETA>= 3.1 && E_probe_ETA < 5.2 cut with efficiency 97.83+/-0.23, pidcut = E_probe_PID_E > 1.5

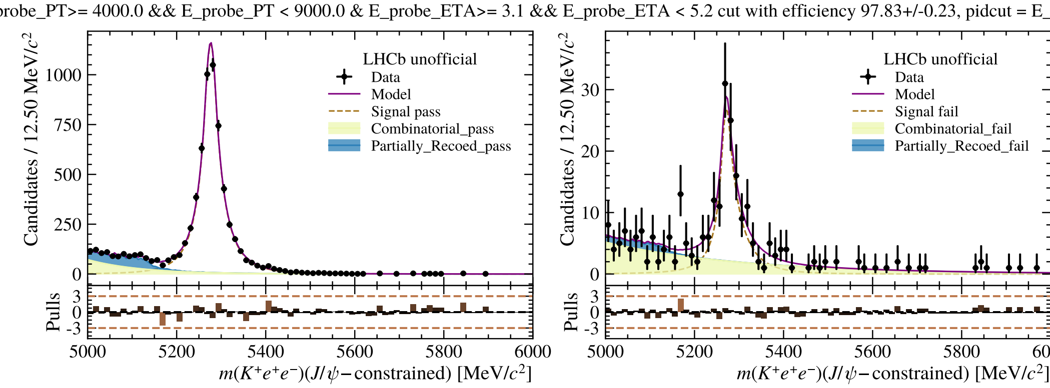

Fig. 75: Fit inbinx-axis-idx=3,y-axis-idx=2

Bin (4,0): E_probe_PT>= 9000.0 && E_probe_PT < 25000.0 & E_probe_ETA>= 1.5 && E_probe_ETA < 2.5 cut with efficiency 98.84+/-0.48, pidcut = E_probe_PID_E > 1.5

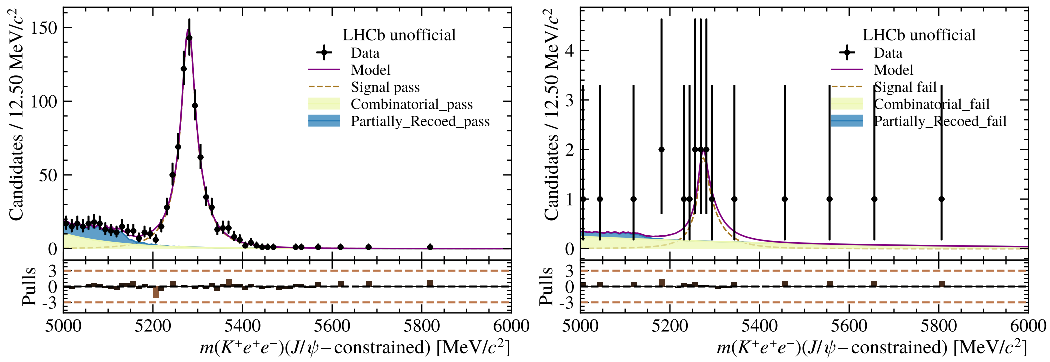

Fig. 76: Fit inbinx-axis-idx=4,y-axis-idx=0

Bin (4,1): E_probe_PT>= 9000.0 && E_probe_PT < 25000.0 & E_probe_ETA>= 2.5 && E_probe_ETA < 3.1 cut with efficiency 97.32+/-0.63, pidcut = E_probe_PID_E > 1.5

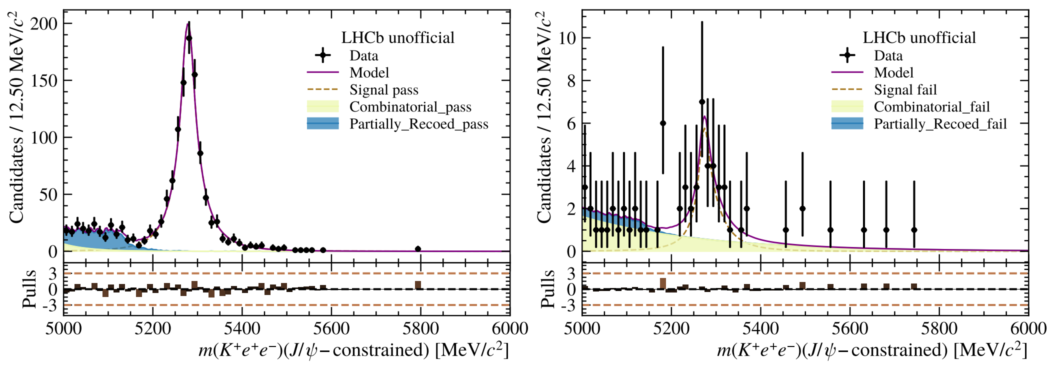

Fig. 77: Fit inbinx-axis-idx=4,y-axis-idx=1

Bin (4,2): E_probe_PT>= 9000.0 && E_probe_PT < 25000.0 & E_probe_ETA>= 3.1 && E_probe_ETA < 5.2 cut with efficiency 97.78+/-0.85, pidcut = E_probe_PID_E > 1.5

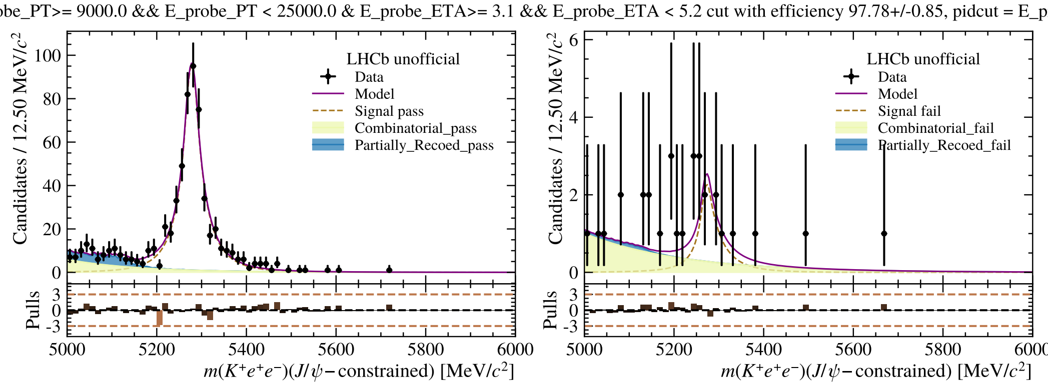

Fig. 78: Fit inbinx-axis-idx=4,y-axis-idx=2

12 Appendix E

Bin (0,0): E_probe_PT>= 500.0 && E_probe_PT < 700.0 & E_probe_ETA>= 1.5 && E_probe_ETA < 2.5 cut with efficiency 87.59+/-4.02, pidcut = E_probe_PID_E > 3

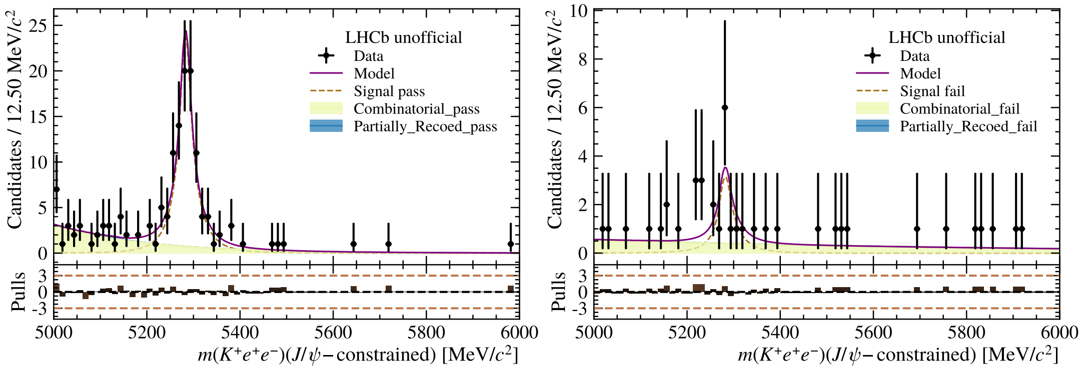

Fig. 79: Fit inbinx-axis-idx=0,y-axis-idx=0

Bin (0,1): E_probe_PT>= 500.0 && E_probe_PT < 700.0 & E_probe_ETA>= 2.5 && E_probe_ETA < 3.1 cut with efficiency 87.64+/-1.57, pidcut = E_probe_PID_E > 3

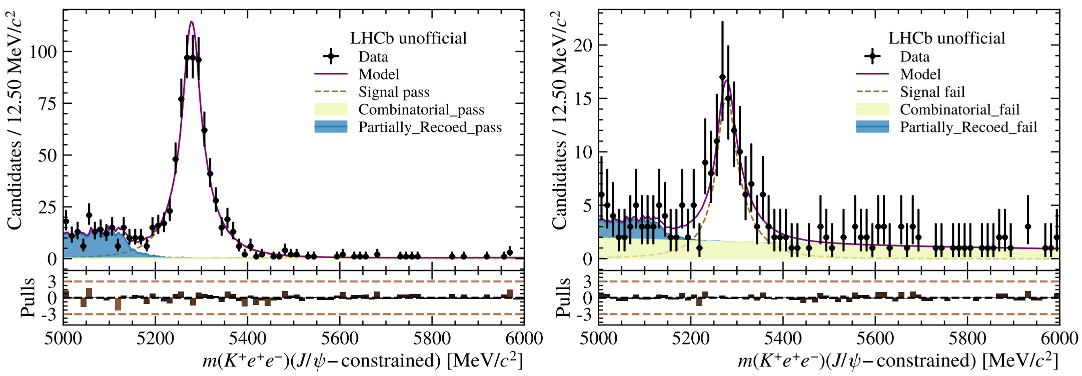

Fig. 80: Fit inbinx-axis-idx=0,y-axis-idx=1

Bin (0,2): E_probe_PT>= 500.0 && E_probe_PT < 700.0 & E_probe_ETA>= 3.1 && E_probe_ETA < 5.2 cut with efficiency 92.11+/-1.09, pidcut = E_probe_PID_E > 3

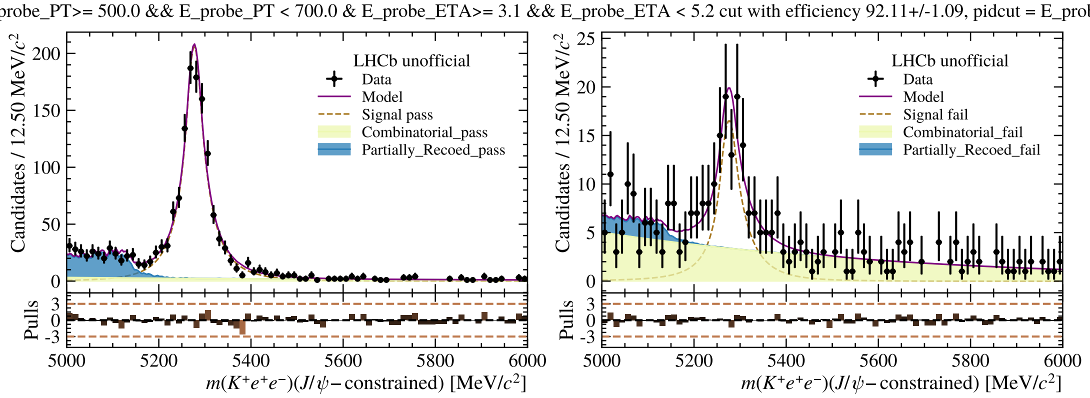

Fig. 81: Fit inbinx-axis-idx=0,y-axis-idx=2

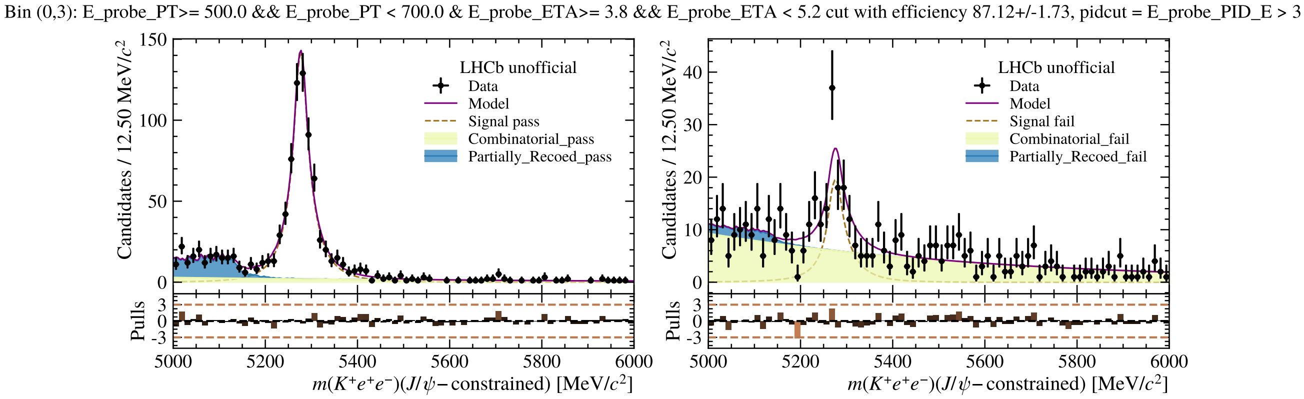

Fig. 82: Fit inbinx-axis-idx=0,y-axis-idx=3

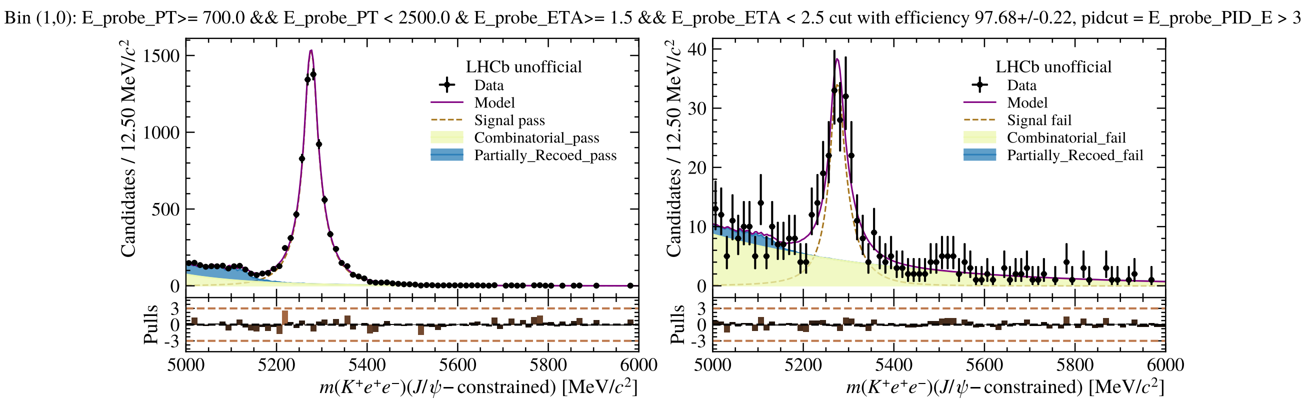

Fig. 83: Fit inbinx-axis-idx=1,y-axis-idx=0

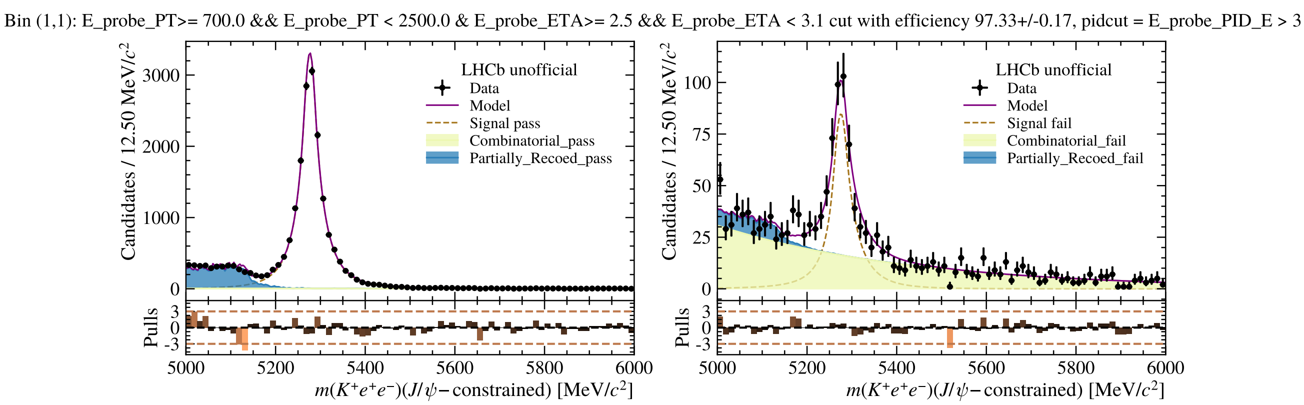

Fig. 84: Fit inbinx-axis-idx=1,y-axis-idx=1

Bin (1,2): E_probe_PT>= 700.0 && E_probe_PT < 2500.0 & E_probe_ETA>= 3.1 && E_probe_ETA < 5.2 cut with efficiency 94.93+/-0.21, pidcut = E_probe_PID_E > 3

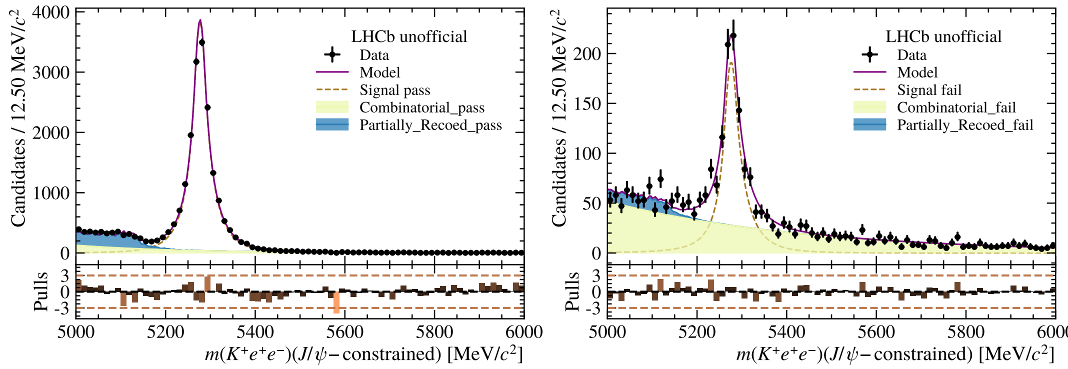

Fig. 85: Fit inbinx-axis-idx=1,y-axis-idx=2

Bin (1,3): E_probe_PT>= 700.0 && E_probe_PT < 2500.0 & E_probe_ETA>= 3.8 && E_probe_ETA < 5.2 cut with efficiency 92.85+/-0.47, pidcut = E_probe_PID_E > 3

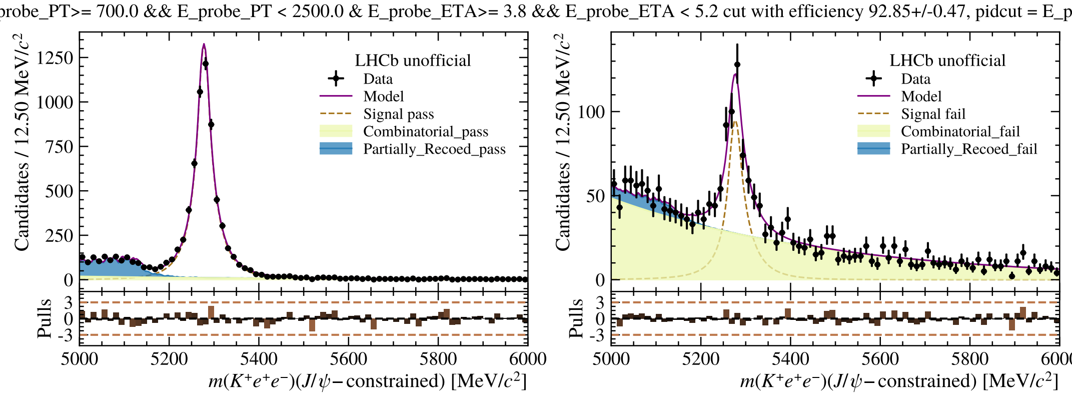

Fig. 86: Fit inbinx-axis-idx=1,y-axis-idx=3

Bin (2,0): E_probe_PT>= 2500.0 && E_probe_PT < 4000.0 & E_probe_ETA>= 1.5 && E_probe_ETA < 2.5 cut with efficiency 98.77+/-0.23, pidcut = E_probe_PID_E > 3

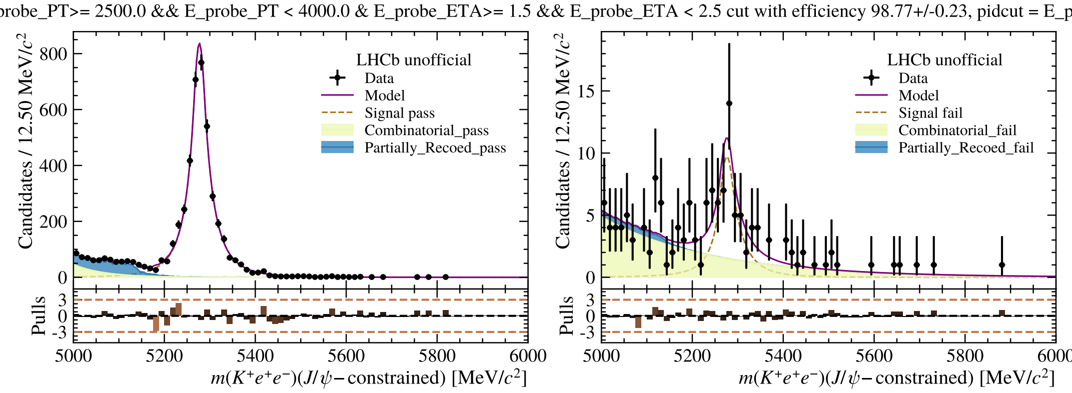

Fig. 87: Fit inbinx-axis-idx=2,y-axis-idx=0

Bin (2,1): E_probe_PT>= 2500.0 && E_probe_PT < 4000.0 & E_probe_ETA>= 2.5 && E_probe_ETA < 3.1 cut with efficiency 97.27+/-0.23, pidcut = E_probe_PID_E > 3

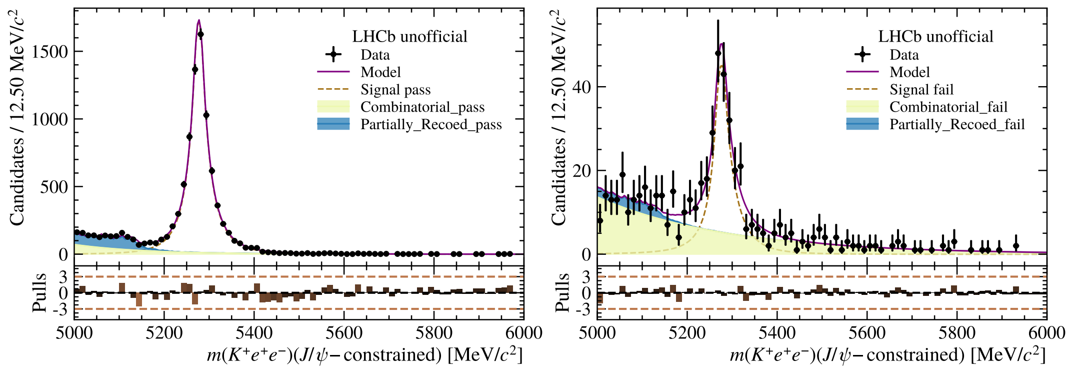

Fig. 88: Fit inbinx-axis-idx=2,y-axis-idx=1

Bin (2,2): E_probe_PT>= 2500.0 && E_probe_PT < 4000.0 & E_probe_ETA>= 3.1 && E_probe_ETA < 5.2 cut with efficiency 96.16+/-0.28, pidcut = E_probe_PID_E > 3

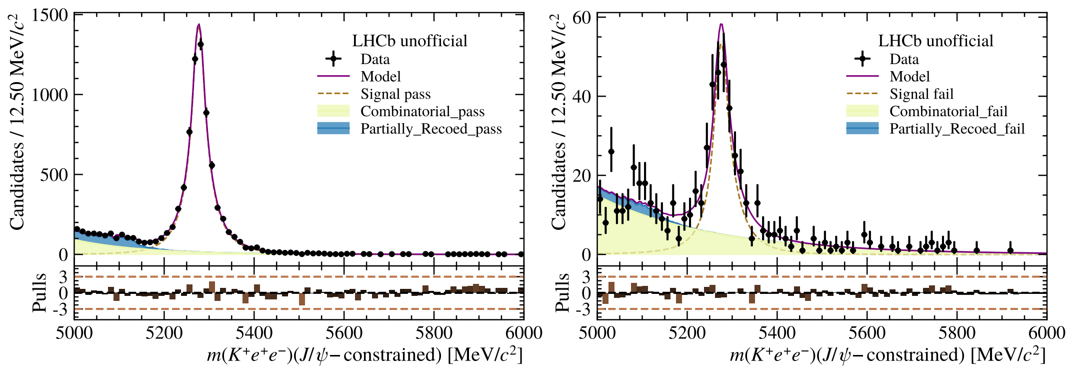

Fig. 89: Fit inbinx-axis-idx=2,y-axis-idx=2

Bin (2,3): E_probe_PT>= 2500.0 && E_probe_PT < 4000.0 & E_probe_ETA>= 3.8 && E_probe_ETA < 5.2 cut with efficiency 95.61+/-0.68, pidcut = E_probe_PID_E > 3

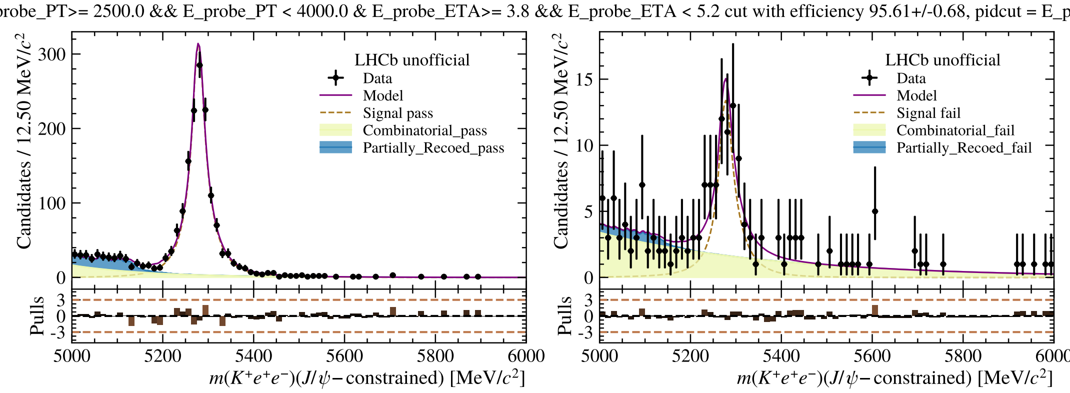

Fig. 90: Fit inbinx-axis-idx=2,y-axis-idx=3

Bin (3,0): E_probe_PT>= 4000.0 && E_probe_PT < 9000.0 & E_probe_ETA>= 1.5 && E_probe_ETA < 2.5 cut with efficiency 97.48+/-0.30, pidcut = E_probe_PID_E > 3

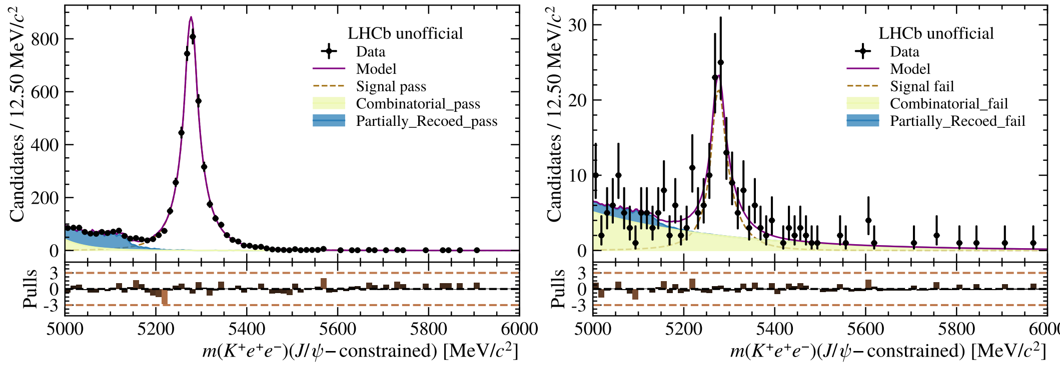

Fig. 91: Fit inbinx-axis-idx=3,y-axis-idx=0

Bin (3,1): E_probe_PT>= 4000.0 && E_probe_PT < 9000.0 & E_probe_ETA>= 2.5 && E_probe_ETA < 3.1 cut with efficiency 96.58+/-0.25, pidcut = E_probe_PID_E > 3

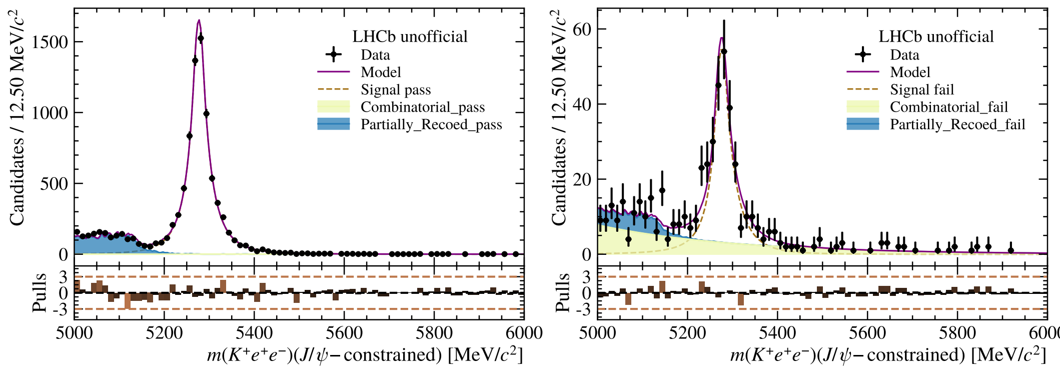

Fig. 92: Fit inbinx-axis-idx=3,y-axis-idx=1

Bin (3,2): E_probe_PT>= 4000.0 && E_probe_PT < 9000.0 & E_probe_ETA>= 3.1 && E_probe_ETA < 5.2 cut with efficiency 96.38+/-0.29, pidcut = E_probe_PID_E > 3

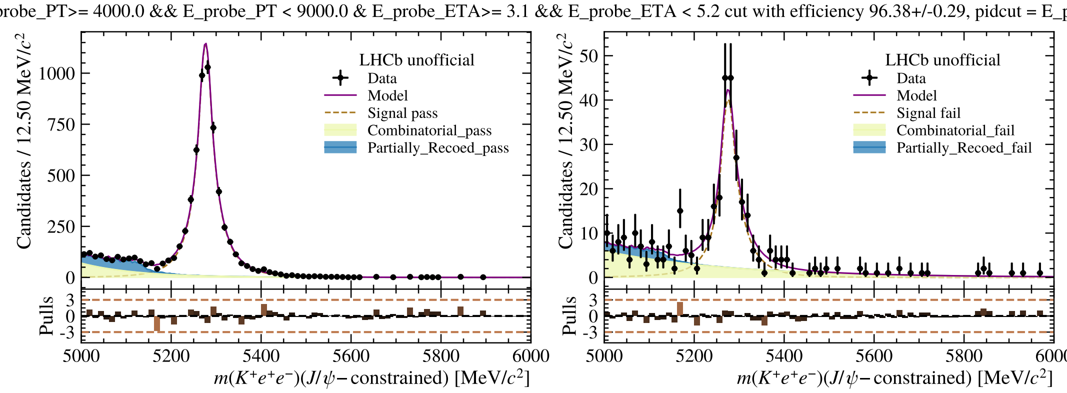

Fig. 93: Fit inbinx-axis-idx=3,y-axis-idx=2

Bin (3,3): E_probe_PT>= 4000.0 && E_probe_PT < 9000.0 & E_probe_ETA>= 3.8 && E_probe_ETA < 5.2 cut with efficiency 96.95+/-0.75, pidcut = E_probe_PID_E > 3

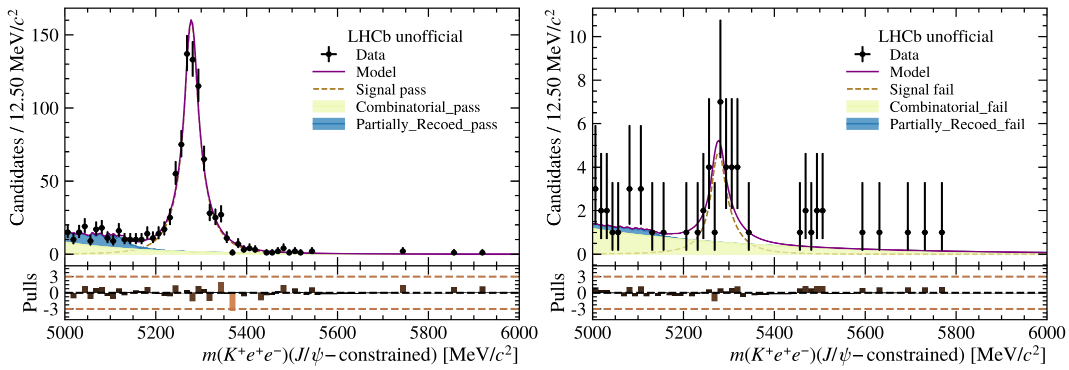

Fig. 94: Fit inbinx-axis-idx=3,y-axis-idx=3

Bin (4,0): E_probe_PT>= 9000.0 && E_probe_PT < 25000.0 & E_probe_ETA>= 1.5 && E_probe_ETA < 2.5 cut with efficiency 98.18+/-0.63, pidcut = E_probe_PID_E > 3

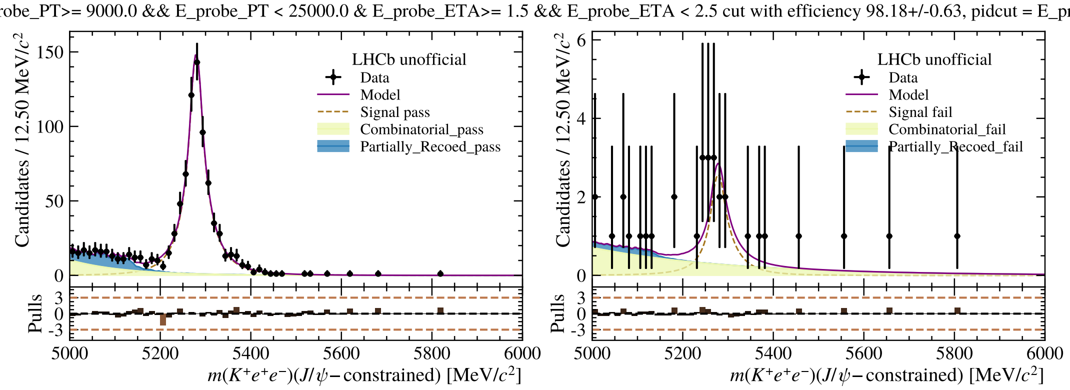

Fig. 95: Fit inbinx-axis-idx=4,y-axis-idx=0

Bin (4,1): E_probe_PT>= 9000.0 && E_probe_PT < 25000.0 & E_probe_ETA>= 2.5 && E_probe_ETA < 3.1 cut with efficiency 96.06+/-0.73, pidcut = E_probe_PID_E > 3

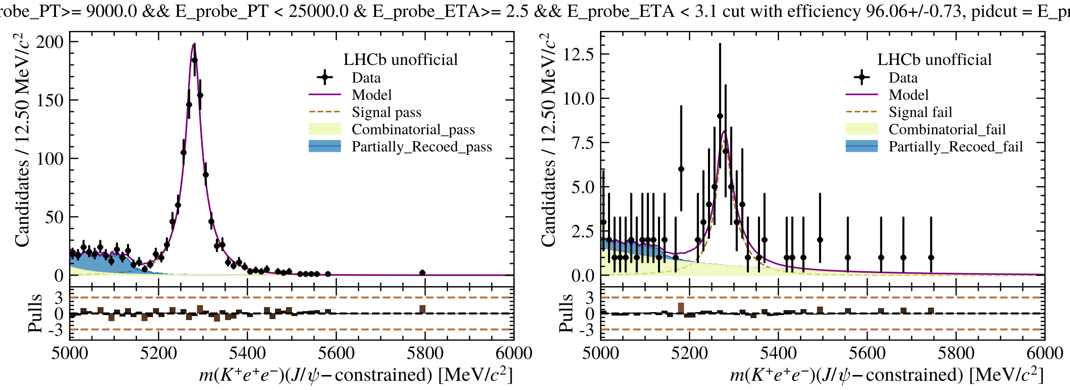

Fig. 96: Fit inbinx-axis-idx=4,y-axis-idx=1

Bin (4,2): E_probe_PT>= 9000.0 && E_probe_PT < 25000.0 & E_probe_ETA>= 3.1 && E_probe_ETA < 5.2 cut with efficiency 96.62+/-0.98, pidcut = E_probe_PID_E > 3

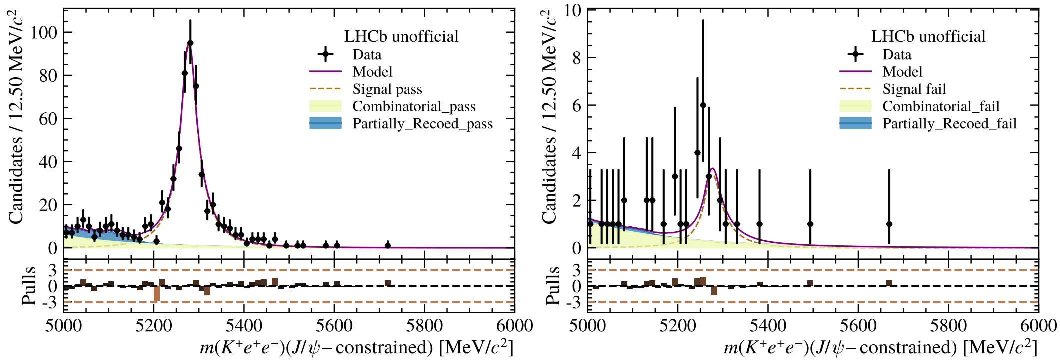

Fig. 97: Fit inbinx-axis-idx=4,y-axis-idx=2

Bin (4,3): E_probe_PT>= 9000.0 && E_probe_PT < 25000.0 & E_probe_ETA>= 3.8 && E_probe_ETA < 5.2 cut with efficiency 98.98+/-1.89, pidcut = E_probe_PID_E > 3

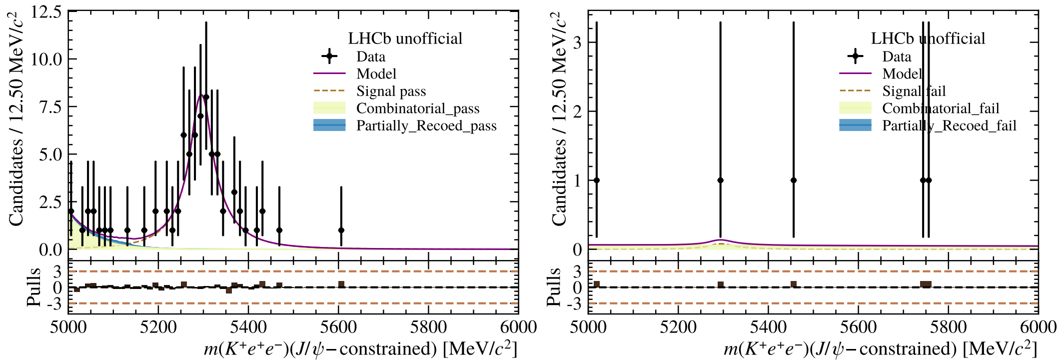

Fig. 98: Fit inbinx-axis-idx=4,y-axis-idx=3